JOURNAL OF PETROLOGY | VOLUME 38 | NUMBER 3 | PAGES 307–336 | 1997

Pressure–Temperature and Fluid Evolution of Quartzo-Feldspathic Metamorphic Rocks with a Relic High-Pressure, Granulite-Facies History from the Central Erzgebirge (Saxony, Germany)

ARNE P. WILLNER[1]*, KERSTIN RÖTZLER[2] AND WALTER V. MARESCH[3]†

[1]INSTITUT FÜR MINERALOGIE, RUHR-UNIVERSITÄT BOCHUM, D-44780 BOCHUM, GERMANY

[2]GEOFORSCHUNGSZENTRUM, TELEGRAPHENBERG, D-14473 POTSDAM, GERMANY

[3]INSTITUT FÜR MINERALOGIE, WESTFÄLISCHE WILHELMS-UNIVERSITÄT, CORRENSSTR. 24, D-48149 MÜNSTER, GERMANY

RECEIVED FEBRUARY 14, 1996 REVISED TYPESCRI*PT* ACCE*PT*ED OCTOBER 7, 1996

The Gneiss–Eclogite Unit is a composite tectonometamorphic unit within the Variscan Erzgebirge mega-antiform. It comprises migmatitic para- and orthogneisses, high-temperature (HT) mylonites, kyanite-bearing granulites, eclogites and garnet peridotites. Four different quartzo-feldspathic assemblages are recognized, in which maximum conditions of up to 830°C and 21 kbar were determined. The assemblages are characterized by the nearly complete prograde breakdown of biotite, by high grossular content (23–47 mol %) of garnet in the presence of albite, and high Si contents of phengite [3·3–3·4 per formula unit (p.f.u.)]. Water activities at this stage are variable and range from <0·15 to >0·4. The maximum pressures indicated for individual rock volumes may vary considerably between 12 and 24 kbar at 700–800°C, so that non-coherency of the entire Gneiss–Eclogite Unit appears likely during the high-pressure event itself. After decompression, concomitant with penetrative HT mylonitization, hydration led to overprinting of the rocks to variable degrees, owing to channelized fluid influx. Partial equilibration at medium-pressure conditions of about 7–10 kbar and 600–700°C occurred, involving abundant retrograde migmatization. The water activity increased to 0·5–1·0. During later exhumation, deformation and re-equilibration at 2–3 kbar and 400–500°C were concentrated in local, discrete, ductile normal fault zones. The kinked geometry of the PT *path is thus characterized by (1) high-pressure (HP) equilibration, followed by near-isothermal decompression at high temperatures, during which rocks from different depths were amalgamated, and (2) extensive hydration and re-equilibration at medium pressures, followed by rapid cooling during continued uplift, when the entire unit came into contact with cooler, now over- and underlying units. This scenario is attributed to continent collision, orogenic collapse and disintegration of the HP unit during continuing collision, crustal stacking and uplift controlled by extension.*

KEY WORDS: *continent collision; fluid evolution; high-pressure granulite facies; PT* history; quartzo-feldspathic rocks

INTRODUCTION

The Erzgebirge is part of the metamorphic basement of the internal Mid-European Variscides exposed in Saxony and the northernmost Czech Republic (Fig. 1). It represents an antiformal megastructure with a large core

*Corresponding author. Present address: Institut für Geowissenschaften, Johannes-Gutenberg-Universität, D-55099 Mainz, Germany.

†Present address: Institut für Mineralogie, Ruhr-Universtät Bochum, D-44780 Bochum, Germany.

composed of medium- to high-grade mica schists and gneisses as well as innumerable intercalations of eclogite from decimetres up to several hundred metres in length. Recently, these eclogites have been studied intensively (Klápová, 1990; Massonne, 1992, 1994; Schmädicke *et al.*, 1992), and it has been found that some record ultra-high-pressure conditions up to 27 kbar and 800°C. Even higher maximum pressures (33–40 kbar; Kotková, 1993; Massonne & Grosch, 1995) have been reported from garnet peridotite lenses that represent remnants of the lithospheric mantle. These contrasting maximum pressures point to a very heterogeneous and strongly incoherent basement. Concurrent petrological work on the quartzo-feldspathic and metapelitic rocks enclosing these eclogite and garnet peridotite lenses also points to high-pressure conditions, although the pressures appear to be considerably lower than in the eclogites and garnet peridotites (Kotková, 1993; Rötzler *et al.*, 1993; Willner *et al.*, 1993, 1994; Rötzler, 1995). In addition, these studies showed that the Erzgebirge consists of a stack of discrete units with contrasting pressure–temperature evolution. Thus the Erzgebirge may be regarded as a model region for studying the continent–continent collision process, especially with regard to the relationships between eclogites and 'normal' crustal rocks enclosing them, as well as the uplift history that resulted in the nappe stack observed today.

This study will concentrate on the quartzo-feldspathic rocks of the Gneiss–Eclogite Unit, exposed in the Central Erzgebirge (Fig. 1). Key occurrences in this unit are small areas with high-temperature (HT) mylonites of granitic composition intercalated parallel to the predominant gneissose foliation. Such rocks preserve not only a relic deformation fabric, but also mineral phases with compositions reflecting an early stage during the metamorphic evolution. Typical are kyanite granulites nearly free of hydrous minerals. These and adjacent rocks were mapped as 'granulitic gneiss' at a scale of 1:25 000 at the turn of the century (e.g. Reinisch, 1929), when initial detailed mapping was done on a purely lithological basis. Definition was primarily based on the characteristic rock fabric. This paper will deal with the petrogenesis of such rocks and the gneisses surrounding them; together they form a discrete tectonic unit in the Central Erzgebirge, the Gneiss–Eclogite Unit. Two major topics will be addressed: (1) high-pressure (HP) metamorphism of a variety of quartzo-feldspathic assemblages under granulite-facies conditions in the uppermost stability field of albite, and (2) the uplift and exhumation process of these rocks, as deduced from an improved understanding of the mechanisms of metamorphic overprinting at high temperatures. In detail, the following set of interrelated problems must be considered:

(1) What are the highest *PT* conditions recorded in quartzo-feldspathic and metapelitic rocks, particularly in the vicinity of eclogites? What happens to these rocks in the extremely wide transitional field involving eclogite, granulite and amphibolite facies? To what extent do both eclogites and adjacent acid rocks have a common history?

(2) Do the quartzo-feldspathic rocks themselves have a common *PT* history? What is the scale of coherence within the high-pressure Gneiss–Eclogite Unit of the Central Erzgebirge?

(3) What are the relationships of the HT mylonite lenses to the surrounding gneisses? Are they relics within an otherwise overprinted coherent unit with a common *PT* history, or are they allochthonous bodies?

(4) What is the role of the metamorphic fluid phase during petrogenesis of the acid metamorphic rocks? What are the specific mechanisms of retrograde overprinting in the quartzo-feldspathic rocks in general?

(5) What information concerning the exhumation history may be derived from the *PT* evolution? Is this *PT* evolution typical for a specific geotectonic environment and how is it related to megascale processes during the Variscan orogenesis?

GEOLOGICAL SETTING

The Erzgebirge antiform structure (Fig. 1) is roughly oval in shape and bounded by the Elbe zone in the east and the Tertiary Eger graben in the south. It is composed of numerous subsidiary dome structures within the medium- to high-grade metamorphic rocks that deform tectonic units with mainly subhorizontal and subparallel transposition foliations. These core rocks are overlain by a phyllitic mantle. The overall 'onion-skin' structure of the entire crystalline complex, as defined by the dominant foliation planes, is a phenomenon that is accepted by all workers in the area. However, although the subhorizontal units of the Erzgebirge were already interpreted as structural units formed by tangential tectonics during the first half of this century (e.g. Kossmat, 1916, 1925; Scheumann, 1935), all later subdivisions for mapping purposes in the 1960s until the 1980s were made on the basis of lithostratigraphic units (e.g. Hoth *et al.*, 1983; Lorenz & Hoth, 1990). These lithostratigraphic units make up rock associations that may be traced along strike for considerable distances. Unfortunately, this subdivisional system was entirely based on an orthostratigraphical philosophy, disregarding clear differences in *PT* conditions between adjacent units and the omnipresent transposition structures of variable age, genesis and displacement character.

In addition, the accepted view until the end of the 1980s was that metamorphic grade gradually increased from the chlorite zone in the outer shell towards anatexis in the core, thus resulting in concentric isograds (Wienholz *et al.*, 1979; Hofmann *et al.*, 1981). Nevertheless, a

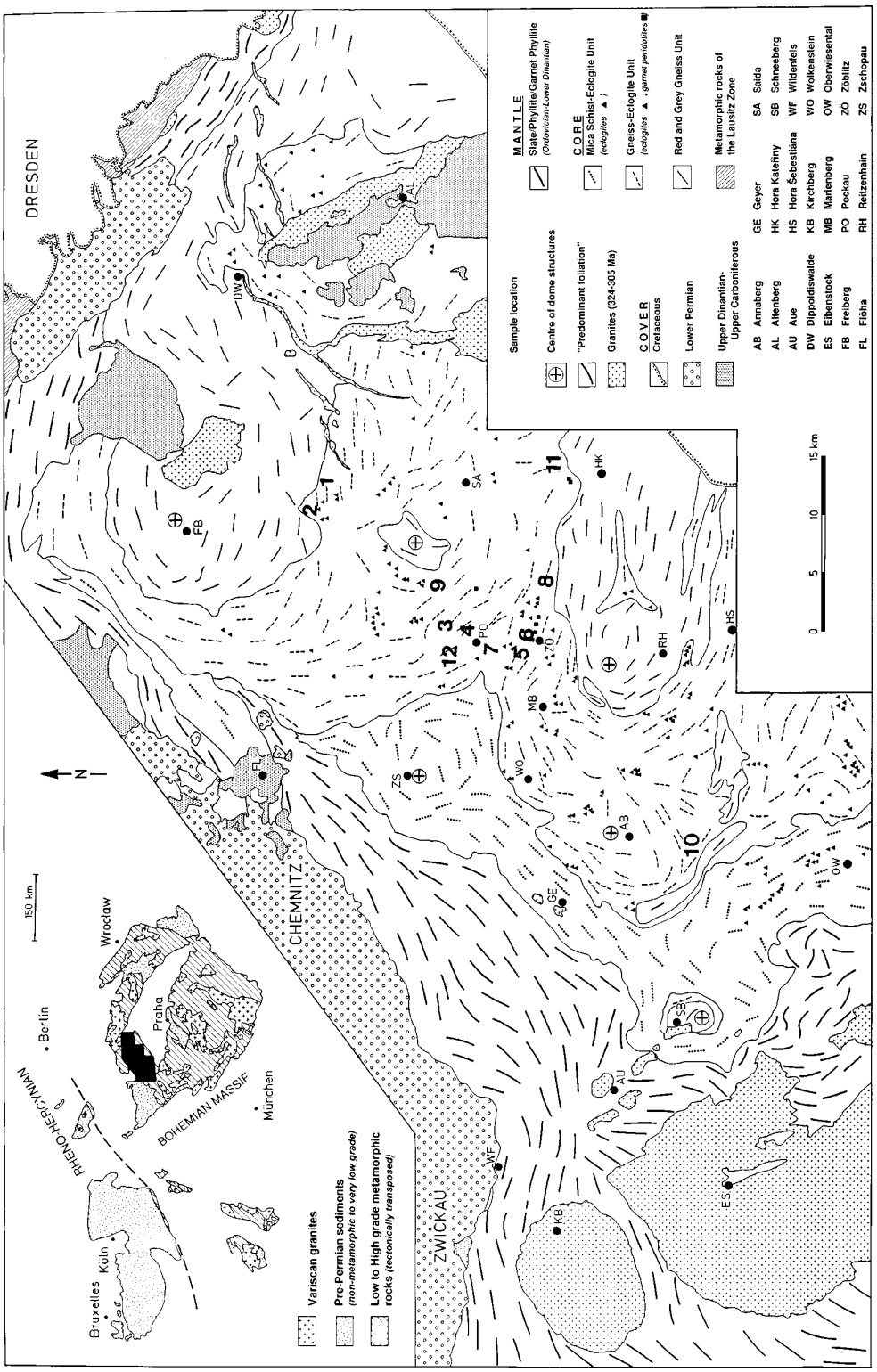

Fig. 1. Geological sketch map of the Erzgebirge based on the geological maps (1:25 000) of Saxony and by Lorenz (1982). Numbers of sample localities refer to Table 1.

remarkably reduced metamorphic profile was observed at the northwestern edge of the mega-antiform. Until the beginning of this decade, metamorphic grade was characterized only by a description of observed assemblages. A first attempt to reconstruct *PT* paths for the Erzgebirge on this basis was made by Krentz *et al.* (1990), who suggested continuously higher pressures towards the core of the mega-antiform. The proposed *PT* loops barely reach the kyanite stability field. A HT–LP imprint well within the sillimanite stability field was recognized in the easternmost part of the Erzgebirge (Bergner, 1990).

However, the first extensive geothermobarometric work revealed that the crystalline Erzgebirge complex was certainly not a coherent body with gradual *PT* variations throughout its history, but rather a stack of subhorizontal structural units with considerable discontinuities in maximum *PT* conditions and markedly di erent *P–T* trajectories. Hence, for the purpose of a better overview, some major units—largely identical to previous major lithostratigraphic units—were summarized and redefined by Willner *et al.* (1994) and Rötzler (1995). The pressure–temperature–deformation histories of these units di er considerably, but even the units themselves cannot be regarded as homogeneous and coherent bodies. From the bottom to the top of the stack these are as follows (Fig. 1):

(1) A 'Grey and Red Gneiss Unit' consists predominantly of monotonous two-mica orthogneisses of granitic composition, with very rare intercalations of garnet amphibolite and metapelite. Eclogites are lacking. Pb–Pb results from zircons with a magmatic morphology yield consistent crystallization ages of 550 Ma for the orthogneisses (Kröner *et al.*, 1995).

(2) The overlying 'Gneiss–Eclogite Unit' is composed of predominantly garnet-bearing ortho- and paragneisses with intercalations of HT eclogite and garnet peridotite. Pb–Pb ages of zircons with magmatic morphology vary around 480 Ma, those of metamorphic zircons around 340 Ma (evaporation method; Kröner & Willner, 1995; Kotková *et al.*, 1996; Willner *et al.*, 1996). Nd–Sm mineral or whole-rock isochrons in HT eclogites and garnet peridotites yield ages between 333 and 360 Ma, interpreted as dating the thermal peak of metamorphism (Schmädicke *et al.*, 1995).

(3) The 'Mica-schist–Eclogite Unit' follows toward the top, where metapelites dominate with abundant intercalated lenses of eclogite, marble, calc-silicate rock and orthogneiss.

(4) The 'Phyllitic Mantle' is composed of slates and phyllites with intercalated quartzite. These rocks represent low-pressure rocks. It is the only unit which contains rocks with known biostratigraphic ages, which range from Silurian to Lower Dinantian (Kurze, 1966), probably also including Ordovician and Cambrian (Freyer *et al.*, 1994). Nevertheless, transposition has also obscured orthostratigraphic relationships in this unit. The contact with the underlying units is a continuous subparallel transposition foliation. Rötzler (1995) identified a separate unit containing garnet phyllites near the contact with the underlying Mica-Schist–Eclogite Unit.

The first pronounced unconformity originated around 325 Ma, when undeformed upper Dinantian clastic sediments were deposited in the NE of the Erzgebirge (Kurze, 1966). This marks the approximate end of the exhumation of the metamorphic core. However, crustal dynamics continued in parts of the now-exposed basement within a near-surface environment, as indicated by pronounced granitic magmatism of crustal anatectic origin intruding rather late (324–305 Ma; Gerstenberger, 1989) into a shallow crustal level (Seltmann *et al.*, 1991). Hence the crustal dynamics recorded by the metamorphic rocks is mainly Variscan and must have occurred, if the geochronological results are correctly interpreted, between 340 and 325 Ma, indicating extremely rapid exhumation rates.

The Gneiss–Eclogite Unit of the Central Erzgebirge features the highest *PT* conditions so far determined, whereas the over- and underlying rock units definitely exhibit lower pressure and temperature histories (Rötzler *et al.*, 1993; Willner *et al.*, 1994, 1995; Klemm, 1995; Rötzler, 1995).

PETROGRAPHY

Small volumes of rock characterized by HT mylonites and facies-critical kyanite granulites are found within the rather homogeneously deformed stack of gneisses that make up most of the Gneiss–Eclogite Unit (e.g. Zöblitz, south of Pockau, Grundau, Saidenbach dam; see Table 1). Lenses of eclogite and garnet peridotite are associated with these occurrences on a regional scale. These rocks are crucial for an understanding of the Gneiss–Eclogite Unit, because here an older deformational fabric and mineral assemblage are preserved that have been obliterated in the surrounding, volumetrically dominant gneisses owing to recrystallization and retrograde overprinting (e.g. Krohe, 1997). A detailed map and a first thorough account of the petrography and microfabrics of such rock association were presented by Behr *et al.* (1965) in the Zöblitz area. Those workers already interpreted the area as part of a deep-seated shear horizon.

The HT mylonites may be almost white, owing to the almost total lack of biotite, and generally show a strong, millimetre-scale foliation. The microfabric is dominated by layers of oriented, large relic quartz and feldspar grains that exhibit marginal recrystallization to variable degrees. Nevertheless, completely homogeneous, strain-free rocks with a polygonal texture—but of comparable

Table 1: Location of analysed samples

1	Ed5a	metablastic gneiss	Lichtenberg, 100 m W of Hornmühle
2	Ed16a	metablastic gneiss	200 m N of Mulda
3	E42g	assemblage 1	Saidenbach dam
	E42-1b	assemblage 1	
	E42i	metablastic gneiss	
4	E43c, e	migmatitic gneiss	Görsdorf Quarry
5	8216	assemblage 1	Burgberg NW of Zöblitz
	E41a	assemblage 1	
6	E3	assemblage 1	Quarry E of Zöblitz
	E726b	assemblage 2	
	E735c	assemblage 3a	
	E726d	assemblage 3a	
	E735a	assemblage 3b	
	E534	assemblage 3b	Morgensternhöhe Ansprung
7	E29a, d, e	assemblage 2	Road cut 500 m S of Pockau
	E28a	metablastic gneiss	
8	E4c	assemblage 3a	500 m NW of Grundau
	E4d	assemblage 3b	
9	E537	assemblage 3b	Mittelsaida
10	E602	assemblage 3a	1 km N of Bärenstein, road to Kühberg
	E36a	assemblage 3a	
11	E47b	metablastic gneiss	Old railway station. Niederlochmühle
12	E45	metablastic gneiss	Rauenstein castle

mineralogy—may also occur intercalated with the HT mylonites on the scale of a few metres. Also on the scale of several metres, the HT mylonites gradually pass into the surrounding overprinted regional gneisses by (1) an increasing degree of recrystallization, (2) a loss of preferred orientation in the quartz domains, and, most prominent, (3) growth of biotite at the expense of garnet and white mica.

For the overprinted regional gneisses we have chosen the term 'metablastic gneiss', as introduced by Mehnert (1968) with reference to migmatized gneiss areas. The term 'metablastesis' describes isochemical recrystallization of an assemblage of minerals at high temperatures. The mineral assemblage can remain unchanged. The emphasis is thus placed on textural rather than mineralogical re-equilibration. We use this term to distinguish overprinted rocks with visible garnet relics from those gneisses free of garnet in which there is no evidence of an equilibration stage before the one now observed and hence no evidence of an overprint or recrystallization. Such 'normal' gneisses without garnet but with abundant white mica and biotite are not considered further in this paper. The metablastic regional gneisses may in part be migmatitic. The planar fabric observed is a mimetic foliation without the relic deformational structures of the HT mylonites. It corresponds to the dominant regional transposition foliation s_2 (Krohe, 1992, 1997; Sebastian, 1995). Rare rootless intrafolial folds may be observed deforming a relic older foliation defined by quartz–feldspar layers (s_1). Kinematic indicators are very rare; they suggest predominant flattening as a major deformational component. A pronounced stretching lineation is oriented east–west to ENE–WSW.

Both the HT mylonites and the surrounding overprinted gneisses are cut by local discrete ductile shear planes with recrystallized quartz, feldspar and white mica. These s_3 planes are generally flat-lying, with normal-fault kinematics and a pronounced ENE–WSW stretching lineation (Krohe, 1997).

Three major peak *PT* assemblages can be distinguished in the HT mylonite domains in quartzo-feldspathic and metapelitic rocks, as follows.

Assemblage 1: quartz + garnet + plagioclase + K-feldspar + kyanite + rutile + (white mica) + (biotite) ± (omphacite)

On the basis of their mineral assemblage, with original prograde white mica being decomposed to potassic feldspar and kyanite, these rocks may be regarded as felsic

granulites. This rock type is rarely foliated and is generally found in small low-strain domains between HT mylonites. Such rocks are characterized by an equigranular polygonal fabric (0·02–0·2 mm) of mainly quartz, K-feldspar, plagioclase and garnet. Some rare, coarser-grained quartz–feldspar veinlets may possibly represent former anatectic melts.

Quartz is the most common matrix phase and is similar in grain size to the feldspars in undeformed rocks. In HT mylonites, layers of small recrystallized quartz grains (<0·02 mm) have formed by recrystallization of a few large elongated individuals (up to 0·2–0·5 mm; 'disc' quartz) with a strong preferred lattice orientation. Quartz also forms inclusions in garnet (orientated inclusion trails), kyanite, plagioclase and potassic feldspar.

Potassic feldspar and plagioclase have variable grain size up to 0·5 mm. The cores of larger K-feldspar grains contain exsolution strings and patches (Fig. 2). In large plagioclase grains, exsolution lamellae are more rarely preserved and mostly developed as patches. However, the rims of all large feldspar grains and all small recrystallized feldspar grains are homogeneous on a microscopic scale. Large deformed augen can also be devoid of exsolution lamellae. In high-strain domains, feldspar porphyroclasts are strongly deformed. Recrystallized grains around their rims are very small (20–100 mm). Subgrain misorientation increases towards the rim of the porphyroclasts (core–mantle structure). Hence, subgrain rotation was an important mechanism of recrystallization.

Garnet is remarkably rich in inclusions, comprising numerous phases such as quartz, kyanite, plagioclase, K-feldspar, rutile, magnetite, pyrite, zircon, monazite and very rare biotite and white mica. Also typical are polycrystalline inclusions predominantly of quartz–K-feldspar–plagioclase and quartz–K-feldspar aggregates that may exhibit symplectitic intergrowth on a cryptocrystalline scale. This type of inclusion is characterized by radial cracks in the surrounding garnet, a feature resembling textures interpreted to be due to the breakdown of coesite inclusions in garnet in Erzgebirge eclogites (Schmädicke *et al.*, 1992). Some garnets show corroded grain boundaries decorated with biotite. In places, garnet forms partial coronas around large plagioclase or kyanite grains.

Kyanite is similar in grain size to all the other matrix minerals; it exhibits preferred orientation and deformation in HT mylonites. Inclusions of white mica, plagioclase, quartz, magnetite, potassic feldspar, monazite and rarely biotite are observed. Garnet, biotite and white mica may survive and replace kyanite.

The amount of biotite observed is generally very low in comparison with typical quartzo-feldspathic assemblages. It is usually absent in the matrix of these rocks, but can occur as 0·2 mm flakes that may in fact be primary. In one sample biotite was observed as an inclusion in garnet and in kyanite. In all other cases biotite represents a retrograde product growing around the rims of garnet and white mica. Some larger biotite grains represent symplectites intergrown with plagioclase.

White mica generally grows around kyanite at the expense of potassic feldspar and kyanite. The degree of this retrograde white mica formation varies strongly. However, rare inclusions in garnet, kyanite and large zircons also indicate the existence of prograde white mica.

Omphacite was observed in one undeformed sample (E42-1b). Fine-grained omphacite–plagioclase symplectites appear to represent pseudomorphs (Fig. 3) that correspond well in shape and size to the surrounding grains of an equigranular polygonal fabric. This suggests that the precursor mineral (clinopyroxene or amphibole) formed part of a dominant assemblage involving plagioclase.

Accessory phases are rutile, magnetite, apatite, zircon and monazite. In HT mylonites rutile and apatite may be aligned within the plane of foliation. Rutile sometimes shows narrow rims of ilmenite. Late rare alteration phases are chlorite, associated with garnet or biotite, and kaolinite replacing kyanite.

Assemblage 2: quartz + garnet + plagioclase + K-feldspar + white mica ± rutile + (biotite) ± (sphene)

Most rocks with this assemblage occur as HT mylonites with features similar to deformed kyanite-bearing granulites, but are characterized by somewhat more pronounced recrystallization. This is probably the precursor rock of most of the regional overprinted gneisses of the Gneiss–Eclogite Unit, which have a similar mineral assemblage, but high and very variable biotite/garnet ratios. Both rock types have a granitic composition, but represent di erent stages of microfabric development.

Again, the microfabric of the HT mylonites is characterized by layers of oriented quartz and feldspar porphyroclasts. Quartz forms augen up to 2·5 mm in size and smaller recrystallized grains of 0·05–0·25 mm. Feldspars are more strongly deformed than those of the kyanite-bearing HT mylonites. Exsolution lamellae are more rarely observed in the feldspar porphyroclasts and are more restricted to the inner cores compared with those of assemblage 1. Both types of feldspar form augen up to 1 mm in size.

Grains of garnet up to 1 mm in diameter contain inclusions of rutile, white mica, plagioclase, K-feldspar, quartz, zircon and K-feldspar–quartz aggregates. They usually have strongly corroded grain boundaries decorated with unoriented biotite. Where the grain boundaries are straight, this is due to an overgrowth of a second

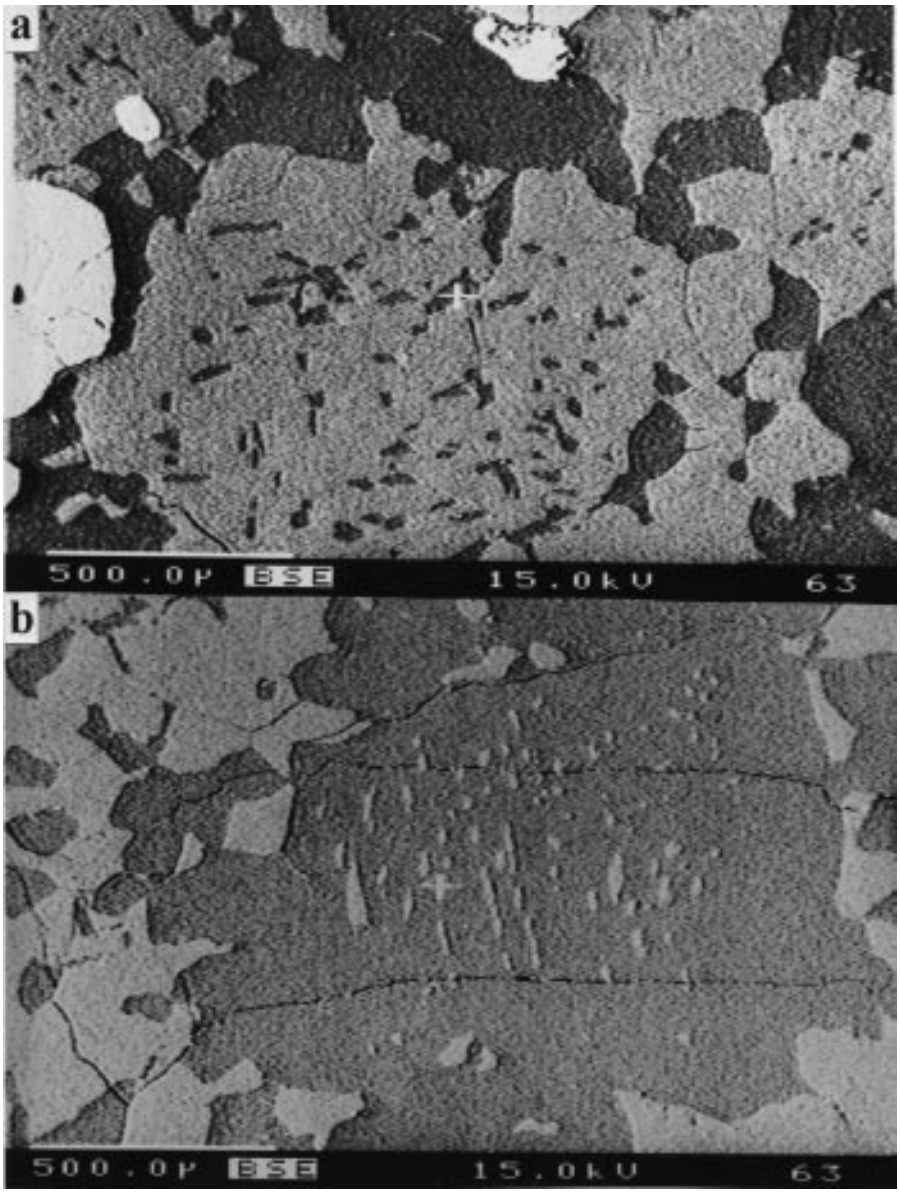

Fig. 2. Back-scattered electron image of (a) perthitic and (b) antiperthitic cores of feldspar grains in a granoblastic kyanite granulite. Sample E42g.

generation of garnet, which may grow along the grain boundaries of coarse matrix phases and enclose retrograde biotite.

White mica is invariably stable in the presence of quartz, and often occurs as inclusions in garnet. In the HT mylonites white mica is often deformed and strongly oriented parallel to the mylonitic foliation (Fig. 4) with a corona of finer-grained biotite, which may be symplectitically intergrown with K-feldspar. Locally, very fine-grained quartz–white mica symplectites also form on the grain boundaries of the white mica.

Biotite is always an unoriented breakdown product of white mica (Fig. 5) and garnet, and may be entirely lacking in some rocks. Similarly, idioblastic unoriented sphene is a retrograde matrix phase with inclusions of round rutile in some samples.

Assemblage 3a: quartz + garnet + white mica + rutile + kyanite ± (ilmenite) ± (biotite); assemblage 3b: quartz + garnet + white mica + rutile + plagioclase ± (ilmenite) ± (biotite)

This rock type is characterized by the total absence of potassic feldspar, a markedly larger grain size compared

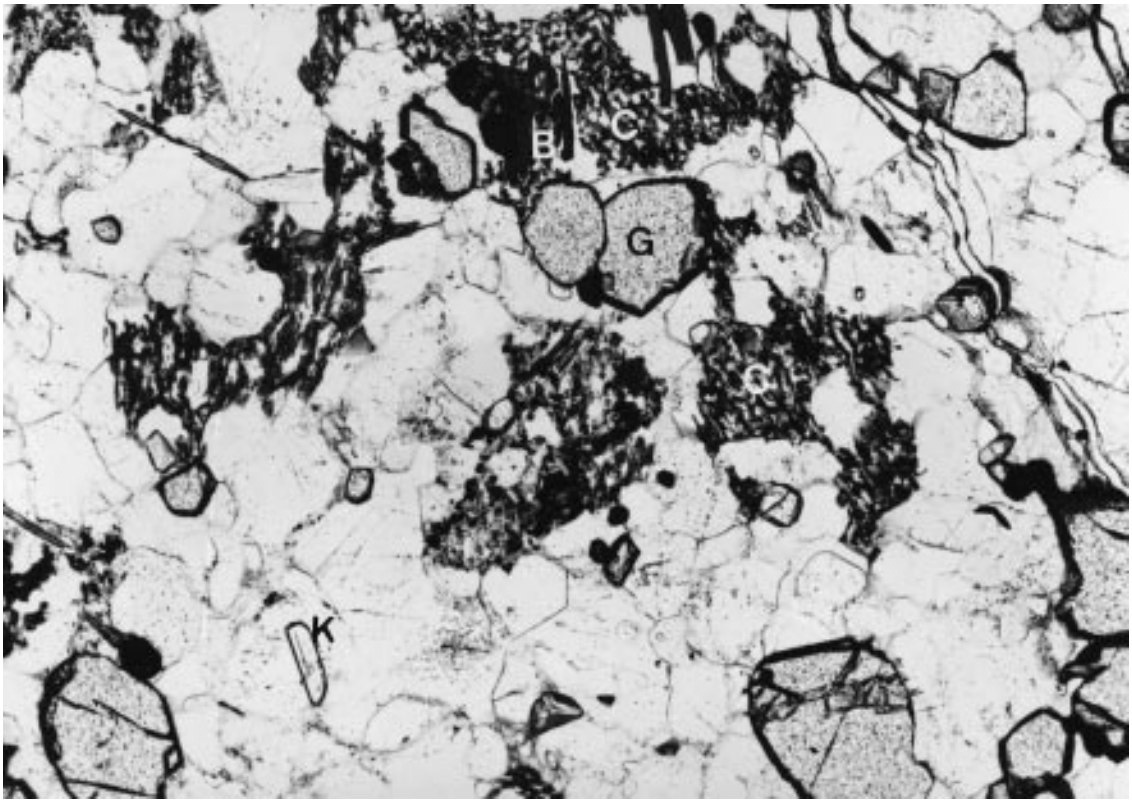

Fig. 3. Clinopyroxene–plagioclase symplectites (C) in a granoblastic matrix with plagioclase, quartz, garnet (G), kyanite (K) and biotite–plagioclase symplectites (B) in a kyanite granulite. Sample E42-1b. Plane-polarized light. Width of photo is 1·75 mm.

with the previous assemblages, and is generally unfoliated or less well foliated owing to pronounced recrystallization. Plagioclase and kyanite are mutually exclusive. On the basis of their mineral content, these rocks may be regarded as metapelites.

Garnet xenoblasts occur with strongly variable grain size ranging from a few millimetres up to several centimetres. The grains are strongly poikiloblastic, containing inclusions of white mica, rutile, kyanite, quartz, pyrite, apatite and very rarely biotite. The cores may be enriched in inclusions, sometimes oriented after a relic foliation or even presenting helicitic trails as a relic internal fabric. Very small oriented needles of rutile form sharply bounded zones that may represent pseudomorphs after a former Ti-rich precursor phase such as biotite. Garnet is locally decomposed to biotite along the rims.

White mica forms conspicuous unoriented crystals up to several millimetres in diameter, or is oriented parallel to the main s_2 foliation as is kyanite. There is no sign that white mica was unstable in the presence of quartz during peak metamorphism. Large xenoblasts of kyanite may be kinked, and contain inclusions of white mica. Some kyanite, on the other hand, is strongly corroded and enclosed in matrix white mica. Both white mica and kyanite may be enclosed in garnet. Some white mica has recrystallized parallel to the local s_3 foliation.

When plagioclase occurs instead of kyanite, it has a grain size and shape similar to matrix quartz (up to a few millimetres), but is also found as an inclusion in garnet. Biotite is an accessory constituent forming occasional narrow rims around white mica, but is also a breakdown product of garnet. The degree of retrograde biotite formation is restricted relative to the K-feldspar-bearing assemblages 1 and 2. Ilmenite forms around abundant matrix rutile; both are enclosed in matrix white mica. Rutile is generally more abundant and larger as an inclusion in garnet. Tourmaline, monazite, apatite and large round zircons are also found among the accessories. Rare magnetite occurs as inclusions in garnet.

Overprinted metablastic gneisses

These are the most widespread rock types in the Gneiss–Eclogite Unit, along with some garnet-free gneiss containing plagioclase, K-feldspar, biotite and white mica in approximately equal amounts. These rocks show a strong increase in the amount and grain size of biotite with respect to the assemblages 1, 2 and 3. In particular, there

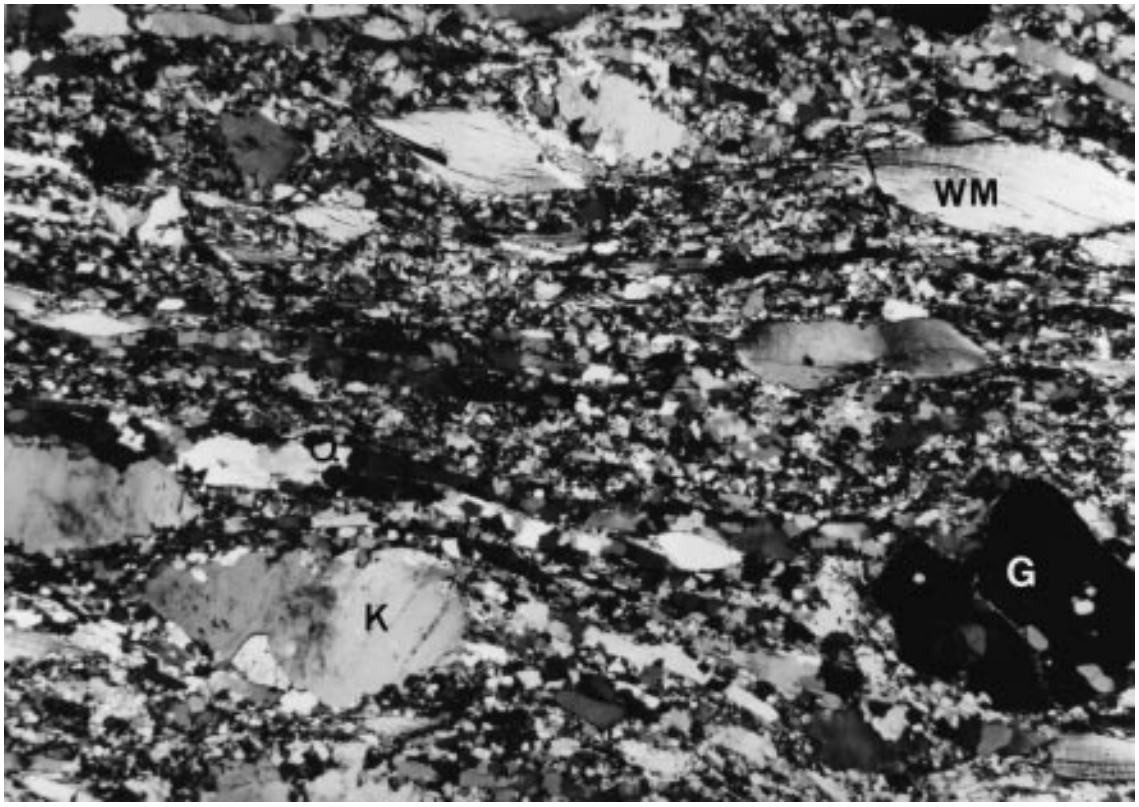

Fig. 4. HT mylonite lacking biotite and with a relic deformation fabric. Deformed white mica (WM), quartz (Q), potassic feldspar (K) and garnet (G) alternate with quartz layers. Sample E726a. Crossed polarizers. Width of photo is 4·5 mm.

may be a continuous transition over only a few metres towards rocks of assemblage 2 , with the biotite/garnet ratio increasing with increasing recrystallization. A strongly planar fabric is still characteristic in hand specimen; asymmetric fabric elements that may be used as shear indicators are generally lacking.

Feldspars and quartz have recrystallized completely, with a strong grain-size variation (0·1–2 mm) owing to recrystallization at high temperatures. Exsolution lamellae in feldspars are rare and observed only in the cores of very large grains. The larger grains may enclose biotite, white mica and corroded garnet. Biotite and white mica have usually recrystallized mimetically within the main s_2 foliation with similar coarse grain size. The strong parallel foliation is mesoscopically identical to the fabric of the HT mylonites. The formation of biotite at the expense of white mica is always clearly discernible and represents the most distinguishing feature of all gneisses in the Gneiss–Eclogite Unit, apart from garnet resorption.

Garnet may show two generations of growth similar to those in the HT mylonites; they are readily distinguished. The older generation is represented by strongly resorbed grains with 2–40 μm inclusions of quartz, K-feldspar, white mica and rutile. In some cases, only accessory relics within biotite flakes are preserved. Garnets of the second generation have straight grain boundaries, enclose coarse matrix quartz and biotite, and tend to form atoll garnets up to 3 mm in diameter. The growth of this garnet obviously occurred along the grain boundaries of the recrystallized biotite-bearing assemblage under static conditions. Sometimes growth of small garnet 2 grains may be observed along the boundaries of large biotites. Occasionally, garnet 1 cores rich in tiny inclusions may be distinguished from garnet 2 rims free of inclusions.

Idioblastic sphene or ilmenite grains are always present, both often containing inclusions of rutile. Small resorbed relics of kyanite may be found occasionally.

Evidence of anatectic partial melting of variable intensity is omnipresent in the metablastic gneisses of the entire Gneiss–Eclogite Unit and may be a dominant feature in some areas [e.g. near Görsdorf and Mulda; see Wienholz *et al.* (1979)]. In some cases, metatexites form, with neosomes of mainly tonalitic and more rarely granitic composition well separated from melanosomes; in other cases, partial melting is more di use. The presence of abundant biotite and white mica in these migmatitic gneisses—also within the neosomes—and the lack of large concentrations of anhydrous minerals such as

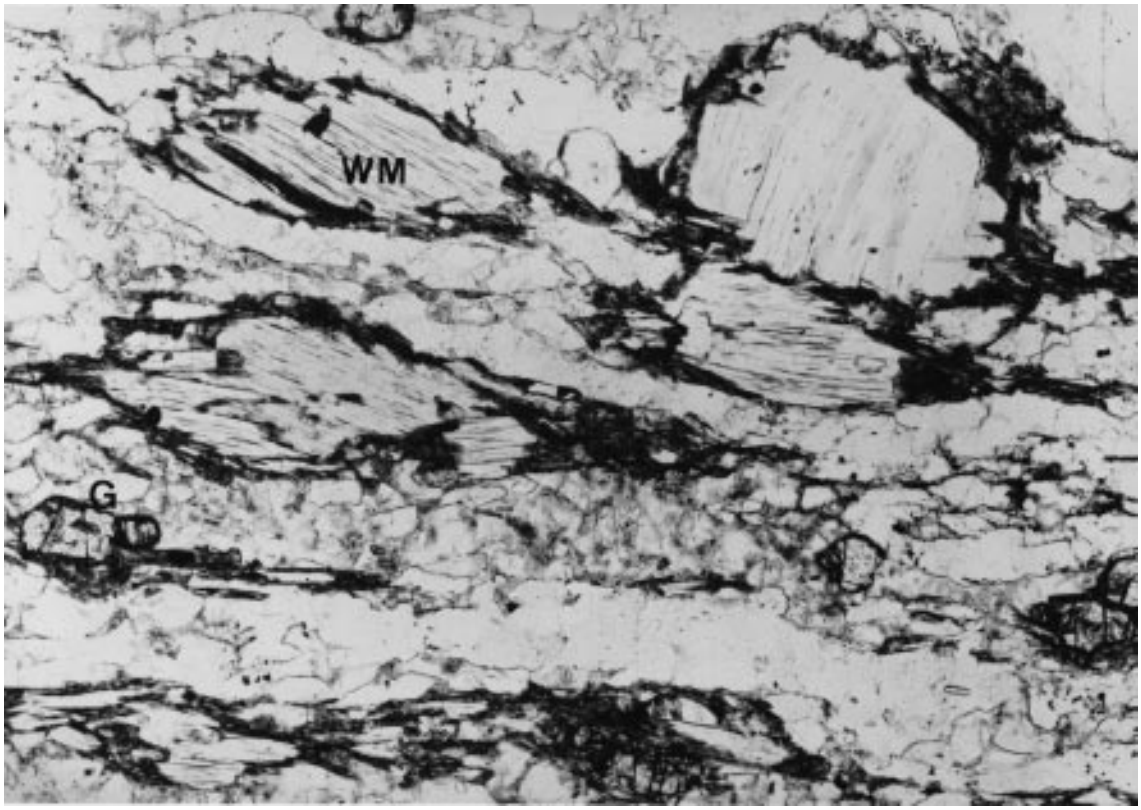

Fig. 5. Fine-grained retrograde biotite grows along the margins of deformed white micas (WM) and garnet (G) in an HT mylonite. Sample E29e. Plane-polarized light. Width of photo is 1·75 mm.

aluminosilicate, garnet, orthopyroxene or cordierite, particularly in the neosomes, indicates anatexis under water-saturated conditions. Coproduction of anhydrous solids together with the melt would be involved.

All rocks of assemblages 1–3, as well as the metablastic gneisses, may show discrete foliation planes of a strongly non-coaxial deformation with normal fault kinematics (D_3; Krohe, 1997). These discrete planes contain recrystallized fine-grained quartz, feldspar and white mica. The formation of green biotite, chlorite and epidote is locally abundant where this late ductile imprint is documented.

MINERAL CHEMISTRY AND ZONING

Analytical methods

Mineral analyses were obtained using electron microprobes (Camebax and Cameca SX50) in Bochum and Potsdam. Operating conditions were 15 kV and 14 nA, with 20 s counting time on peaks and a slightly defocused electron beam to minimize alkali loss when measuring micas or feldspars. The following minerals and synthetic materials were used as standards: andradite glass (Ca, Fe), pyrope (Si, Al, Mg), jadeite (Na), topaz (F), spessartine (Mn), NaCl (Cl), K-silicate glass and rutile (Ti). Representative point analyses are given Tables 2–4. A complete list may be obtained from the first author upon request.

Before turning to geothermobarometric calculations, extensive studies of mineral inhomogeneities must be undertaken to allow the correlation of small domains with particular stages of equilibration. For this purpose, qualitative digital element distribution maps were used extensively. Such maps were produced by measuring X-ray impulses for 2 s per point during a two-dimensional scan across a grain. The data were subsequently processed with appropriate software (Bernhardt *et al.*, 1995). Three elements were usually measured simultaneously. Quantitative line scans were also used. Individual grains of all minerals within most samples were studied in this manner. With this procedure it was possible to select core compositions unequivocally, despite the fact that zoning is asymmetrical in all phases. Particular care was taken to analyse inclusion phases.

Garnet

Garnet composition varies strongly among the di erent assemblages (Fig. 6; Table 2): unusually high grossular

Table 2: Representative compositions of garnet

	E42-1b			E29e			E43e		E736a		E735a	
	core	rim	grt2	core	rim	grt2	grt1	grt2	core	rim	core	rim
SiO_2	37·84	38·07	38·46	36·94	37·16	37·53	37·00	37·38	36·87	37·13	36·60	37·08
TiO_2	0·16	0·07	0·09	0·14	0·12	0·08	0·37	0·09	0·08	0·02	0·13	0·00
Al_2O_3	21·44	21·68	21·79	20·77	20·97	21·21	20·51	20·98	20·61	20·88	20·73	21·05
Cr_2O_3	0·00	0·02	0·04	0·03	0·04	0·01	0·00	0·00	0·00	0·00	0·03	0·01
Fe_2O_3	0·91	0·55	0·54	1·43	0·84	0·99	1·55	1·76	0·94	0·85	0·97	0·91
FeO	25·63	25·06	23·60	25·17	27·98	25·46	30·56	21·83	35·17	36·33	38·66	36·83
MnO	0·45	0·47	0·34	1·69	0·63	0·72	0·83	0·72	1·47	0·38	0·34	0·25
MgO	4·74	5·63	6·04	1·34	2·11	1·64	1·56	0·95	1·99	3·48	2·49	3·63
CaO	8·93	8·13	9·13	12·33	9·87	12·87	8·39	16·89	3·37	1·51	0·82	1·24
Sum	100·10	99·68	99·93	99·84	99·72	100·51	100·77	100·60	100·50	100·68	100·77	101·00
Cations based on 24 O												
Si	5·920	5·938	5·949	5·898	5·934	5·925	5·909	5·887	5·954	5·951	5·915	5·920
Al^{IV}	0·080	0·062	0·051	0·102	0·066	0·075	0·091	0·113	0·046	0·049	0·085	0·080
Al^{VI}	3·874	3·923	3·921	3·808	3·880	3·873	3·769	3·780	3·877	3·895	3·863	3·882
Cr	0·000	0·003	0·005	0·004	0·004	0·001	0·000	0·000	0·000	0·000	0·004	0·001
Fe^{3+}	0·107	0·065	0·063	0·172	0·101	0·117	0·187	0·209	0·113	0·103	0·118	0·117
Ti	0·019	0·009	0·011	0·016	0·015	0·009	0·044	0·011	0·010	0·002	0·015	0·000
Sum	4·000	4·000	4·000	4·000	4·000	4·000	4·000	4·000	4·000	4·000	4·000	4·000
Mg	1·106	1·310	1·394	0·319	0·502	0·385	0·372	0·223	0·480	0·831	0·601	0·864
Fe^{2+}	3·353	3·269	3·053	3·361	3·736	3·362	4·082	2·875	4·749	4·869	5·225	4·917
Mn	0·059	0·062	0·045	0·228	0·085	0·096	0·113	0·096	0·201	0·051	0·047	0·034
Ca	1·497	1·359	1·513	2·110	1·689	2·177	1·435	2·850	0·582	0·259	0·142	0·212
Sum	6·015	6·000	6·005	6·018	6·012	6·020	6·002	6·044	6·012	6·010	6·015	6·027

Table 3: Representative compositions of feldspar, pyroxene and sphene

	Plagioclase						
	E42-1b			E28e			E43e
	I*	IIC	IIR	I*	IIC	IIR	
SiO_2		65·83	66·92	65·32	65·90	67·30	64·56
Al_2O_3	20·82	21·59	22·81	20·95	20·78	22·29	21·88
Fe_2O_3	0·00	0·03	0·03	0·00	0·06	0·03	0·07
BaO	0·06	0·00	0·02	0·00	0·03	0·03	0·06
CaO	2·41	2·09	3·26	1·90	1·59	3·16	2·63
Na_2O	9·04	9·83	9·85	9·46	10·58	9·61	10·03
K_2O	2·41	0·36	0·19	1·78	0·35	0·14	0·26
Sum	100·00	100·86	101·52	100·00	100·73	100·01	100·39
Cations based on 8 O							
Si	2·914	2·909	2·837	2·910	2·933	2·846	2·871
Al	1·086	1·106	1·168	1·090	1·067	1·158	1·131
Fe^{3+}	0·000	0·001	0·001	0·000	0·002	0·001	0·003
Sum	4·000	4·016	4·006	4·000	4·002	4·005	4·005
Ba	0·001	0·000	0·000	0·000	0·001	0·001	0·001
Ca	0·087	0·097	0·152	0·090	0·074	0·149	0·124
Na	0·776	0·828	0·828	0·810	0·894	0·821	0·853
K	0·136	0·020	0·011	0·100	0·019	0·008	0·015
Sum	1·000	0·945	0·991	1·000	0·988	0·979	0·992

	Potassic feldspar					Clinopyroxene		Sphene	
	E42-1b		E29e		E43e	E42–1b			
	I*	II	I*	II					
SiO_2	64·96	62·87	65·22	64·51	63·82	SiO_2	53·71	SiO_2	29·83
Al_2O_3	19·04	19·11	18·79	18·43	18·75	TiO_2	0·26	TiO_2	33·59
Fe_2O_3	0·00	0·04	0·00	0·03	0·03	Al_2O_3	11·17	Al_2O_3	3·79
BaO	0·50	0·54	0·11	0·16	0·41	FeO	5·88	Fe_2O_3	0·53
CaO	0·37	0·08	0·24	0·00	0·00	MgO	7·60	CaO	28·29
Na_2O	2·98	1·72	2·41	1·15	1·18	CaO	15·61	H_2O	0·18
K_2O	12·15	13·64	13·22	15·43	15·20	Na_2O	4·89	F	1·17
Sum	100·00	98·03	100·00	99·91	99·40	Sum	99·02	Sum	96·90
Cations based on 8 O						*Cations based on 6 O*			
Si	2·973	2·955	3·086	2·988	2·972	Si	1·949	Si	0·991
Al	1·027	1·058	1·014	1·006	1·029	Al^{IV}	0·051	Ti	0·839
Fe^{3+}	0·000	0·001	0·000	0·001	0·001			Al	0·147
Sum	4·000	4·014	4·000	3·995	4·002	Al^{VI}	0·427	Fe^{3+}	0·011
						Ti	0·007	Ca	1·007
Ba	0·008	0·010	0·002	0·003	0·008	Fe	0·179	OH	0·042
Ca	0·019	0·004	0·012	0·000	0·000	Mg	0·411	F	0·116
Na	0·264	0·157	0·214	0·104	0·107	Ca	0·607		
K	0·709	0·818	0·772	0·912	0·903	Na	0·344	O†	4·834
Sum	1·000	0·989	1·000	1·018	1·017	Sum	1·975		

*Composition integrated (see text); C, core; R, rim.
†Three cations; $OH = (Al + Fe^{3+}) - F$; $O = [(\Sigma \text{ positive valencies}) - OH - F]/2$.

Table 4: Representative mineral analyses of micas

	White mica												
	E42-1b	E42g in Zc	E42g in Ky	E29e in Grt	E29e core	E29e rim	E29a WM III	E736a in Grt	E736a core	E736a rim	E735a in Grt	E735a core	E43e
SiO_2	47·09	47·21	46·27	49·97	48·37	47·74	44·91	50·52	49·59	49·29	49·64	47·98	48·63
TiO_2	2·46	2·61	0·31	0·90	1·43	0·89	0·13	0·37	0·29	0·41	0·86	1·58	0·69
Al_2O_3	29·33	28·29	39·98	29·28	27·89	29·07	32·12	28·37	27·38	30·02	28·00	29·91	29·19
Cr_2O_3	0·04	0·04	0·00	0·01	0·06	0·02	0·00	0·05	0·03	0·08	0·03	0·02	0·00
FeO	2·62	1·54	0·40	3·21	3·95	3·87	4·72	2·55	2·57	1·98	2·46	2·59	4·48
MnO	0·00	0·03	0·01	0·03	0·03	0·02	0·03	0·00	0·06	0·01	0·00	0·03	0·02
MgO	2·40	3·55	0·29	2·88	2·25	2·00	1·87	2·82	2·76	2·20	2·66	1·82	2·51
CaO	0·00	0·00	0·52	0·04	0·00	0·00	0·00	0·00	0·00	0·00	0·00	0·00	0·00
BaO	0·56	0·34	0·00	0·14	0·11	0·00	0·00	0·11	0·17	0·23	0·15	0·17	0·19
Na_2O	0·31	0·45	6·49	0·19	0·20	0·23	0·19	0·56	0·29	0·59	0·38	0·47	0·15
K_2O	10·65	10·73	1·82	9·72	11·04	10·92	10·59	9·90	10·39	9·93	10·72	10·74	10·76
F	0·00	0·49	0·15	0·47	0·59	0·55	0·60	0·10	0·14	0·11	0·15	0·05	0·03
Cl	0·05	0·03	0·00	0·01	0·00	0·00	0·00	0·02	0·04	0·01	0·04	0·02	0·00
H_2O	4·43	4·19	4·63	4·33	4·16	4·16	4·10	4·45	4·32	4·42	4·37	4·43	4·47
Sum*	99·93	99·41	100·83	101·01	99·86	99·27	98·59	99·76	97·95	99·23	99·37	99·78	101·16
Ions based on 22 O													
Si	6·362	6·392	5·903	6·601	6·560	6·497	6·171	6·736	6·764	6·601	6·685	6·457	6·504
Al^{IV}	1·638	1·608	2·097	1·399	1·440	1·503	1·829	1·264	1·236	1·399	1·315	1·543	1·496
Al^{VI}	3·033	3·907	3·914	3·159	3·018	3·160	3·372	3·193	3·164	3·340	3·130	3·200	3·105
Ti	0·250	0·266	0·030	0·090	0·146	0·091	0·013	0·037	0·004	0·041	0·087	0·160	0·070
Cr	0·004	0·005	0·000	0·001	0·007	0·002	0·000	0·006	0·030	0·008	0·003	0·002	0·000
Fe	0·297	0·174	0·043	0·355	0·448	0·440	0·493	0·284	0·293	0·221	0·277	0·292	0·501
Mn	0·003	0·003	0·001	0·004	0·003	0·002	0·004	0·000	0·007	0·001	0·000	0·003	0·002
Mg	0·483	0·716	0·054	0·566	0·454	0·406	0·383	0·561	0·560	0·440	0·534	0·365	0·500
Sum	4·070	4·071	4·042	4·175	4·078	4·106	4·265	4·080	4·058	4·051	4·031	4·023	4·178
Ca	0·000	0·000	0·070	0·005	0·000	0·000	0·000	0·000	0·000	0·000	0·000	0·000	0·000
Ba	0·030	0·018	0·000	0·008	0·006	0·000	0·000	0·006	0·009	0·012	0·008	0·003	0·010
Na	0·081	0·119	1·605	0·048	0·054	0·059	0·050	0·144	0·077	0·154	0·100	0·115	0·040
K	1·836	1·853	0·297	1·639	1·909	1·895	1·857	1·684	1·807	1·696	1·841	1·858	1·835
Sum	1·947	1·990	1·972	1·700	1·969	1·954	1·907	1·834	1·893	1·862	1·949	1·976	1·885
F	0·000	0·209	0·059	0·184	0·237	0·222	0·243	0·042	0·060	0·047	0·064	0·022	0·014
Cl	0·011	0·007	0·000	0·001	0·000	0·000	0·001	0·005	0·008	0·002	0·008	0·004	0·000
OH	3·989	3·784	3·941	3·815	3·763	3·778	3·756	3·954	3·932	3·951	3·928	3·974	3·987

*Sum corrected for fluorine.

Table 4: continued

	White mica			
	E42-1b	E3 in Ky	E29e in Grt2	E43e
SiO_2	36·24	38·41	36·44	35·54
TiO_2	3·77	3·10	3·47	2·05
Al_2O_3	13·78	17·05	15·80	17·62
Cr_2O_3	0·00	0·10	0·00	0·03
FeO	18·54	11·01	20·58	23·33
MnO	0·05	0·03	0·06	0·19
MgO	11·60	16·13	8·34	6·77
CaO	0·02	0·00	0·07	0·00
BaO	0·34	n.d.	0·09	0·08
Na_2O	0·10	0·13	0·04	0·07
K_2O	9·33	9·34	9·92	9·39
F	0·47	n.d.	0·88	0·21
Cl	0·48	n.d.	0·24	0·03
H_2O	3·52	4·12	3·40	3·74
Sum*	98·11	99·42	98·90	99·04
Ions based on 22 O				
Si	5·628	5·592	5·638	5·536
Al^{IV}	2·372	2·408	2·362	2·464
Al^{VI}	0·151	0·517	0·520	0·771
Ti	0·441	0·295	0·404	0·240
Cr	0·000	0·012	0·000	0·003
Fe	2·408	1·340	2·663	3·039
Mn	0·006	0·003	0·007	0·025
Mg	2·684	3·502	1·923	1·572
Sum	5·690	5·669	5·519	5·650
Ca	0·004	0·000	0·011	0·000
Ba	0·020	0·000	0·006	0·005
Na	0·030	0·036	0·013	0·021
K	1·848	1·735	1·957	1·865
Sum	1·902	1·771	1·987	1·891
F	0·232	n.d.	0·433	0·009
Cl	0·126	n.d.	0·062	0·103
OH	3·643	4·000	3·505	3·888

Table 5: Mineral abbreviations

Ab	albite	Ky	kyanite
Ace	Mg-aluminium celadonite	L	melt
Alm	almandine	Ms	muscovite
An	anorthite	Or	orthoclase
And	andalusite	Phe	phengite
Ann	annite	Phl	phlogopite
Bt	biotite	Plag	plagioclase
Cpx	clinopyroxene	Py	pyrope
Di	diopside	Qtz	quartz
Grs	grossular	Rt	rutile
Grt	garnet	Sil	sillimanite
Ilm	ilmenite	V	vapour
Jad	jadeite	WM	white mica
Kfs	potassic feldspar		

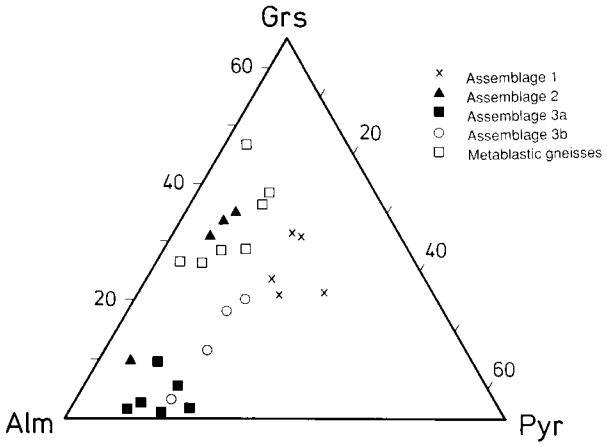

Fig. 6. Grossular–almandine–pyrope ratios of garnet core compositions.

contents characterize garnet core compositions of assemblages 1 (22–33 mol %), 2 (10–35 mol %) and 3b (10–20 mol %), and the metablastic gneisses (25–45 mol %), in contrast to those of the feldspar-free assemblage 3a (<5 mol %).

Assemblage 1 has particularly pyrope-rich garnets (20–33 mol %), in contrast to all other white-mica-bearing assemblages (5–15 mol %). Whereas almandine contents are generally 50–70 mol % in most assemblages, the feldspar-free assemblage 3a in particular has very almandine-rich garnets (80–92 mol %), owing to an Fe- and Al-rich whole-rock chemistry. Spessartine contents are minor in all assemblages, generally below 2 mol %, but rarely up to 7 mol %.

Conspicuous and very irregular zoning of garnet is a consistent feature with similar characteristics in all assemblages (Fig. 7). Most typical is a strong decrease of the grossular component from the core towards the corroded rim. Zoning roughly follows the shape of the corrosion embayments, indicating that it cannot represent a prograde growth feature. The second generation of garnet has idioblastic grain boundaries and discontinuously overgrows the irregular rims of the resorbed garnets of the first generation. It is characterized by a strong increase in Ca content. This garnet generation is present in all rocks, but in di ering amounts. In weakly overprinted rocks it is only detectable by two-dimensional

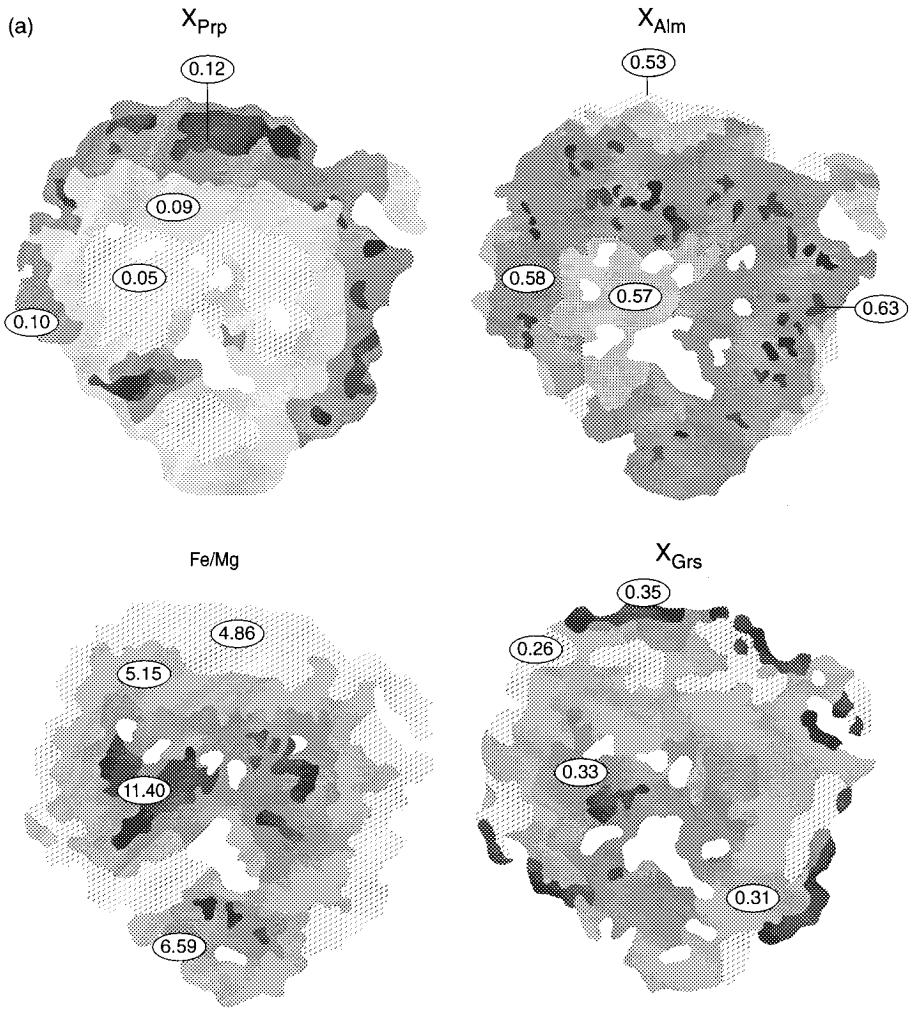

Fig. 7.

element distribution mapping. The boundaries between the two garnets are generally sharp, but may be somewhat transitional in some cases. There may also be a slight decrease of the grossular component towards the rim of the second garnet generation. In strongly overprinted gneisses this generally atoll-shaped idioblastic second generation dominates; small, irregular relics of the corroded first generation (Fig. 7b) may be distinguished only by careful element distribution mapping.

Fe contents generally decrease and Mg contents increase toward the garnet rims. Fe/(Fe + Mg) always decreases continuously from core to rim, more or less concentrically with respect to the grain boundaries, even across the boundaries between the two garnet generations. This may be seen in all assemblages. Only in the outermost rims, especially of the second-generation garnet in the metablastic gneisses, does the trend reverse again. Mn is either unzoned or decreases slightly from core to rim. In general, compositions of small garnets are equivalent to rim compositions of large grains.

Plagioclase

In fresh, unaltered samples of all plagioclase-bearing assemblages 1, 2 and 3b (Table 3) the core composition is albite ($An_{7–11}$). The Ca content increases continuously towards the rim ($An_{11–15}$). The zoning is very asymmetrical (Fig. 8a). Patches in the outermost rim or in very small matrix grains may contain up to 20–36 mol % anorthite component. In metablastic gneisses, anorthite contents may increase from 10 to 30 mol % from the cores toward the rims. Rare antiperthitic cores in some larger grains, especially in assemblages 1 and 2, allow reconstruction of an earliest plagioclase composition (Table 3). Normally, inclusions of plagioclase in garnet are also albite with up

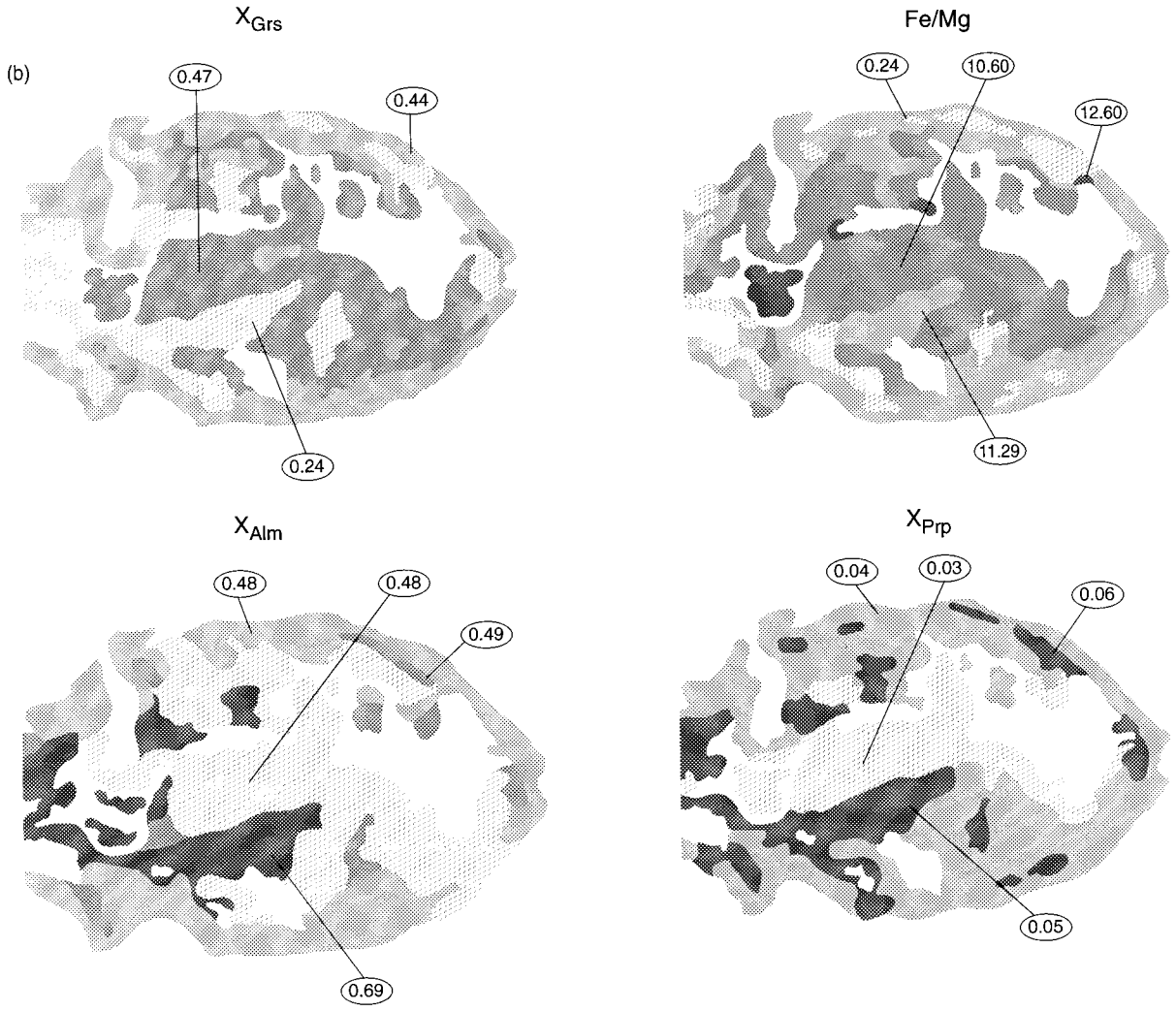

Fig. 7. Characteristic element distribution maps of garnet in (a) assemblage 2 (E29e) and (b) overprinted metablastic gneiss (E43e).

to 10 mol % anorthite component. Rare exceptions are oligoclase (An_{20}) inclusions in garnet of assemblages 1 and 2.

K-feldspar

K-feldspar has a remarkably uniform composition in all assemblages (88–92 mol % orthoclase component; Table 3), both in homogeneous as well as in perthitic grains. However, the integrated composition of the perthitic cores in larger grains reveals an original composition near the temperature peak with ~71–77 mol % orthoclase component (Table 3).

White mica

The composition of white mica may vary slightly from assemblage to assemblage, but most strongly from one generation to the next (Table 4). In general, contents of Si [>3·2 per formula unit (p.f.u.)] and Ti (>0·03 p.f.u.) are enhanced; Mg contents always exceed those of Fe, whereas the paragonite content is <5 mol %. Al contents are generally somewhat lower than expected according to the Tschermak substitution, indicating some ferri-muscovite component.

Zoning is omnipresent, strongly asymmetric and irregular, with Si and Ti contents decreasing near the rim, whereas Al increases (Fig. 8b). Mg/(Mg + Fe) (0·55–0·75) and Na/(Na + K) (0·04–0·08) generally show no systematic variation from core to rim, but decreasing Mg/(Mg + Fe) and increasing Na/(Na + K) are occasionally observed.

Two generations are clearly detectable in assemblage 1. Relic prograde white mica can be found in garnet, kyanite or zircon, occasionally with high Si contents

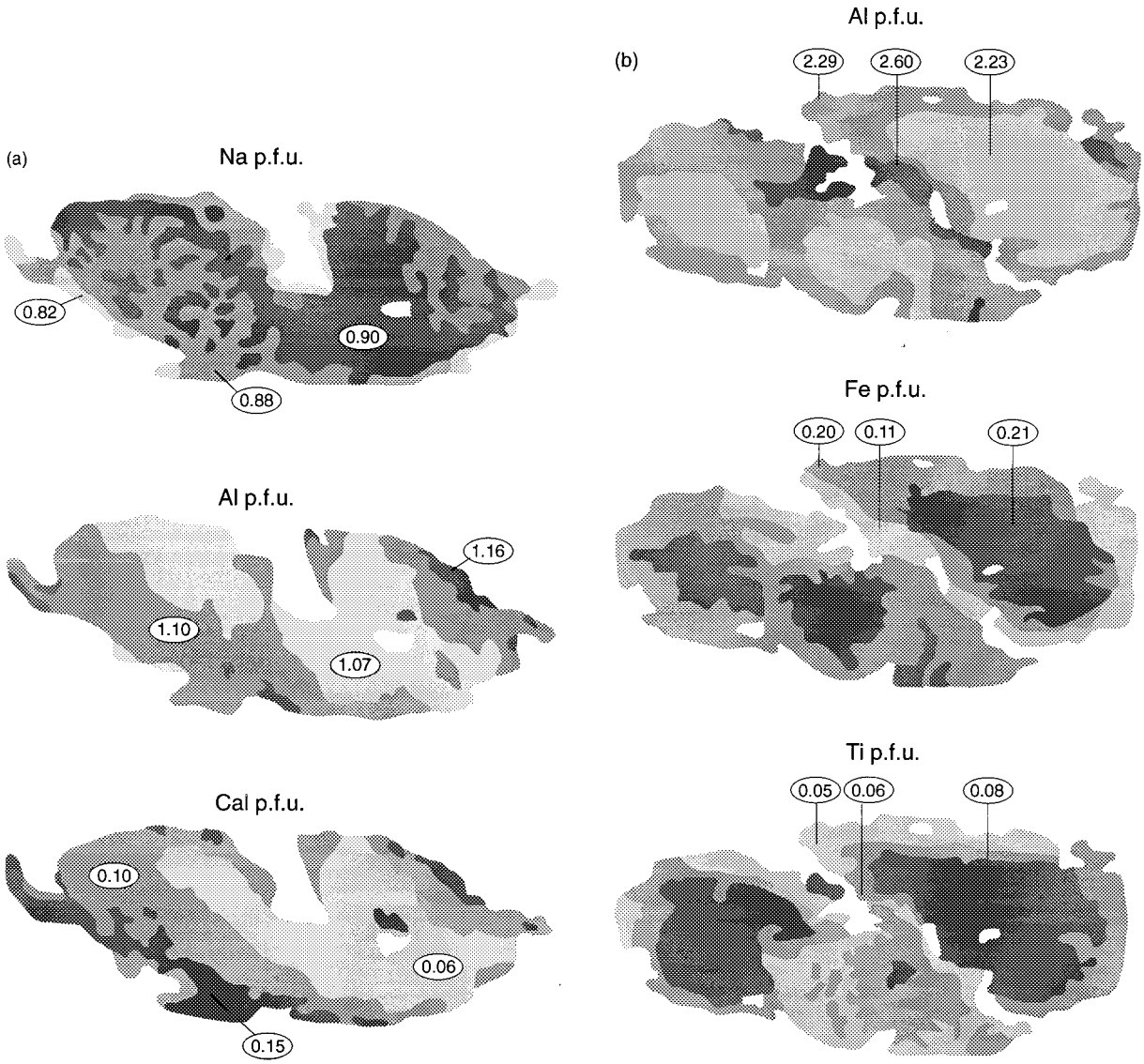

Fig. 8. Characteristic element distribution maps of (a) plagioclase; (b) white mica from assemblage 2 (E29e).

(3·2–3·35 p.f.u.). The Na contents may also be high (6–9 mol %), and paragonite was also found. Mg/(Mg + Fe) tends to be higher than in the matrix white mica. White mica inclusions are more abundant in assemblages 2 and 3 as well as in metablastic gneisses. In assemblage 2 their composition is comparable with that of the cores of matrix white mica. As in the metablastic gneisses, Si contents in assemblage 2 micas vary from 3·2 to 3·3 p.f.u. with a strong decrease to 3·15 Si p.f.u. near the rims, and Ti contents range from 0·06 to 0·12 p.f.u.

In white micas of assemblages 3a and 3b, di erences between included and matrix white mica are always evident. The included white mica consistently shows lower Ti but higher Si and Na contents. The composition of the included and matrix white mica varies considerably (Si 3·15–3·4 p.f.u.; Ti 0·02–0·1 p.f.u.) among di erent samples.

In all the various assemblages, fine-grained white mica of a late third generation grew parallel to discrete, ductile normal shear planes (Krohe, 1997). This generation exhibits significantly lower Si and Ti contents (3·07–3·14 Si p.f.u.; 0·02–0·04 Ti p.f.u.) with identical compositions in all assemblages.

Omphacite

Omphacite is only known from symplectites in one sample of assemblage 1; it has a continuously variable

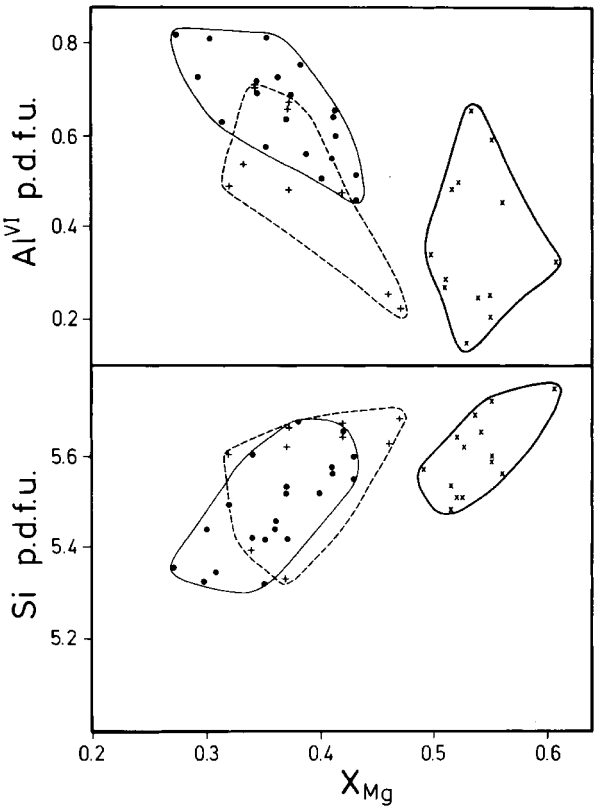

Fig. 9. Al^{VI} and Si vs X_{Mg} = Mg/(Mg + Fe) variations in biotite of selected rocks of assemblage 1 (×, E42-1b) and assemblage 2 (●, E29a; +, E29d).

composition from 20 to 34 mol % jadeite component. Plagioclase in these symplectites is richer in An (14 mol %) than the cores of the matrix plagioclase.

Biotite

Biotite compositions (Table 4) vary considerably, even within single grains. However, variations within single grains are not systematic. Only in strongly overprinted gneisses do biotite compositions tend to be more uniform. Mg/(Mg + Fe) varies between assemblages, being more magnesian in assemblage 1 (0·45–0·65) than in assemblage 2 (0·25–0·45), whereas biotites from assemblages 3a and 3b cover the complete spectrum. However, the latter are considerably higher in Al content (>0·4 p.f.u). Very rare inclusions of biotite in garnet 1 have lower Mg/(Mg + Fe) values than the respective matrix biotite.

In three samples a noticeable statistical tendency for a decrease in Si and an increase in AlVI with decreasing Mg/(Mg + Fe) was found (Fig. 9). Both e ects should reflect consistent continuous changes of *PT* conditions. Ti contents are relatively high (0·05–0·2 p.f.u.), similar to those found in other HT rocks (Schreurs, 1985), but do not show any regular variation. Remarkably high chlorine contents of 0·01–0·08 p.f.u. were detected in all relict, non-overprinted assemblages, which strongly exceed those of biotites from amphibolite-facies gneisses (<0·005 p.f.u.; Willner, 1994). Biotites from overprinted gneisses always have low Cl contents.

Sphene

Sphene particularly occurs in rocks of assemblage 1, showing considerable contents of F (0·08–0·17 p.f.u.) that correspond to increased Al contents according to the substitution $Ti^{4+} + O^{2-} = Al^{3+} + F^{-}$ (Table 3).

PHASE RELATIONSHIPS

A notable feature of all quartzo-feldspathic rocks studied is the total absence of epidote, even as an inclusion mineral, except as a late retrograde alteration product. Epidote was observed by Le Go & Ballèvre (1990), who studied high-pressure granitic orthogneisses characterized by the breakdown of the anorthite component in plagioclase to form Ca-rich garnets as in the quartzo-feldspathic rocks considered here. Those workers suggested that epidote should be stable in such assemblages below ~600°C. Hence our samples must have formed well above the stability field of epidote–biotite–quartz as delineated by Le Go & Ballèvre (1990).

Furthermore, the evolution of the present quartzo-feldspathic rocks is dominated by the nearly complete breakdown of prograde biotite toward peak metamorphic conditions, and retrograde growth of new biotite. The HT mylonitization is bracketed by an early biotite-absent assemblage containing plagioclase, K-feldspar, quartz and kyanite or white mica, and a retrograde assemblage always containing biotite and white mica. Phase relationships at such HP–HT conditions may be illustrated by petrogenetic grids for the KMASH and KCMASH systems, involving the phases phlogopite, pyrope, potassic feldspar, quartz, kyanite, muscovite, Al-celadonite, grossular and anorthite (Figs 10 and 11). These phases exist as components of solid solutions in the rocks considered and the reactions shown are therefore multivariant and continuous over a very large *PT* field. Prominent is the continuous breakdown of biotite in the presence of quartz and kyanite or white mica towards high temperature and high pressure.

The three major biotite-absent assemblages may represent di erent water activities at constant pressure and temperature (Fig. 10). The water-dependent reactions a ecting the fields of the three assemblages are

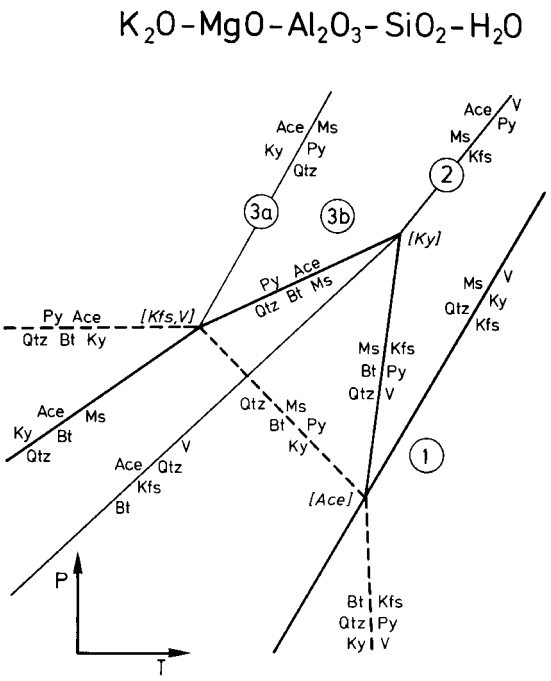

Fig. 10. Schematic partial *PT* grid involving the mineral components Al-celadonite, muscovite, pyrope, quartz, phlogopite, kyanite and K-feldspar in the system K_2O–MgO–Al_2O_3–SiO_2–H_2O. Numbers refer to assemblages 1–3 (see text). Bold lines mark the upper stability of biotite + muscovite, dashed lines that of biotite + kyanite.

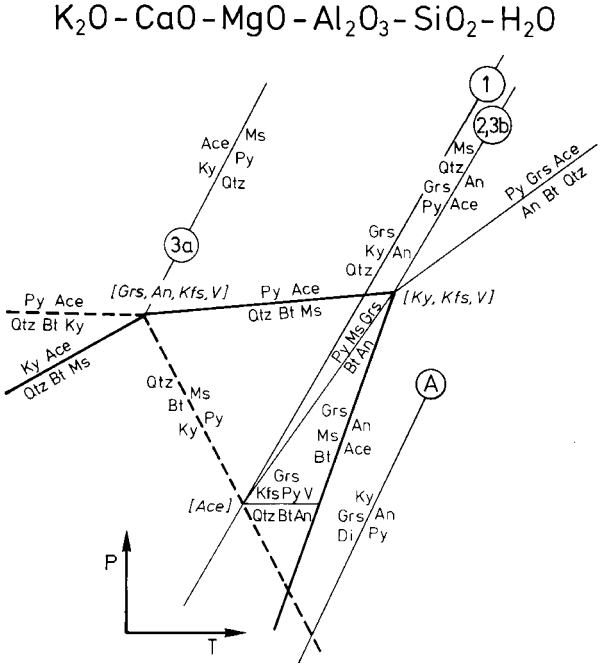

Fig. 11. Schematic partial *PT* grid involving the mineral components Al-celadonite, muscovite, pyrope, grossular, anorthite, quartz, phlogopite, kyanite and K-feldspar in the system K_2O–CaO–MgO–Al_2O_3–SiO_2–H_2O. Numbers refer to assemblages 1–3 (see text). Additional reaction A including diopside is placed relatively to the proposed grid. Bold lines mark the upper stability of biotite + muscovite, dashed lines that of biotite + kyanite.

$$Ms_{WM} + Qtz = Or_{Kfs} + Ky + H_2O \quad (1)$$

and

$$3Ms_{WM} + Ace_{WM} = 4Or_{Kfs} + Py_{Grt} + 4H_2O. \quad (2)$$

Both reactions may be used as hygrometers. At given *PT* conditions and comparable whole-rock compositions, water activity decreases from assemblage 3 towards 1 in the KMASH system (Fig. 10). The AFM plot in Fig. 12a shows the alternative assemblages 1 and 2 for rocks with very similar bulk rock composition that may be an e ect of variable water activity. Notable is the strong shift in garnet composition owing to complete breakdown of phengite in assemblage 1.

The K-feldspar-free assemblage 3 may involve either kyanite or plagioclase (assemblage 3a or 3b, respectively). In the KCMASH system (Fig. 11) both assemblages are separated by the multivariant reaction

$$Grs_{Grt} + 2Ky + Qtz = 3An_{Plag} \quad (3)$$

which may serve as a barometer for assemblage 1. Assemblages 2 and 3b are defined by the continuous barometer reaction

$$2Grs_{Grt} + Py_{Grt} + 6Qtz + 3Ms_{WM} = \quad (4)$$

$$6An_{Plag} + 3Ace_{WM}$$

and assemblage 3a by

$$3Ace_{WM} + 4Ky = 3Ms_{WM} + Py_{Grt} + 4Qtz. \quad (5)$$

Jadeitic clinopyroxene is a retrograde phase in only one sample of assemblage 1. The principal occurrence of jadeitic clinopyroxene below the pure end-member reaction

$$Jad + Qtz = Ab \quad (6)$$

depends on the stability of a diopside component in clinopyroxene. Where anorthite and grossular coexist as Ca-bearing phase components, coexistence of an additional diopside component at equilibrium is governed by the multivariant reaction

$$3Di_{Cpx} + Grs_{Grt} + 6Ky = Py_{Grt} + 6An_{Plag}. \quad (7)$$

Such a reaction occurs only in assemblage 1. However, this assemblage contains additional quartz. Hence, to overlap with the multivariant reaction (3), the pyrope component in garnet must be low relative to the grossular component (Fig. 11). Otherwise, the anorthite component in plagioclase would have to be absent in rocks containing

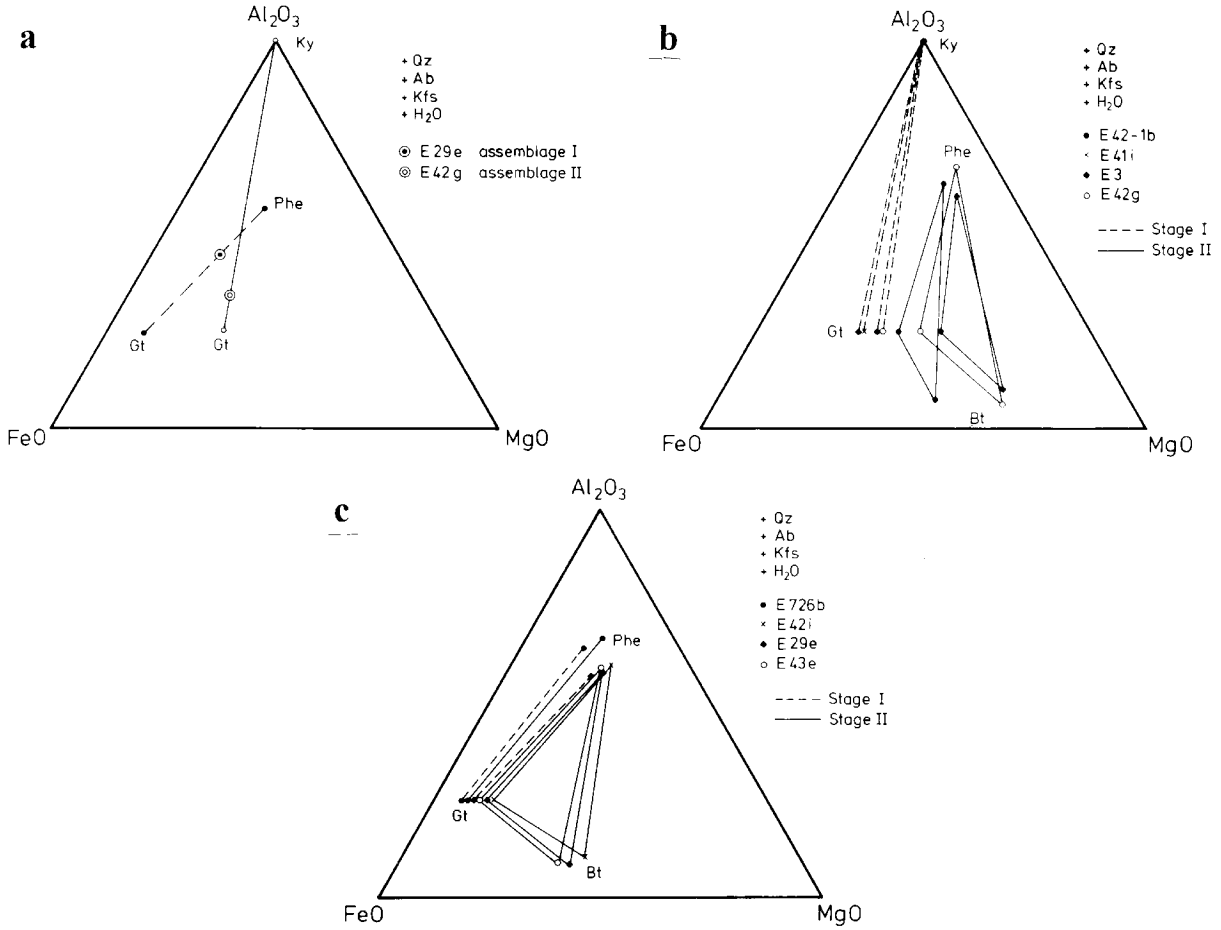

Fig. 12. Projections of the phase compositions of assemblages 1 and 2 in AFM diagrams from quartz, K-feldspar, albite and H_2O for two successive equilibration stages: (a) the alternative assemblages 1 and 2 for HP–HT stage I caused by variable water activities; (b) assemblage 1 compositions for the HP–HT stage I and a retrograde stage II in local rock domains; (c) as in (b), for assemblage 2.

grossular-rich garnet to stabilize diopside at elevated pressure.

Whereas the biotite-absent assemblages are defined by whole-rock chemistry (e.g. Fig. 12a), retrograde phengite–garnet–biotite assemblages form under static conditions to variable degrees by reaction and equilibration in local rock domains (Fig 12b). The retrograde reactions involve simultaneous dehydration and hydration reactions. For instance, the breakdown of the Al-celadonite component in phengite by decompression will release water (Fig. 10):

$$3Ace_{WM} = Phl_{Bt} + 2Or_{Kfs} + 3Qtz + 2H_2O \quad (8)$$

whereas growth of biotite by pressure or temperature release generally involves addition of water (Figs. 10 and 11):

$$Grs_{Grt} + 2Py_{Grt} + 2Or_{Kfs} + 2H_2O = 2Phl_{Bt} + 3An_{Plag} + 3Qtz \quad (9)$$

$$Ms_{WM} + Phl_{Bt} + 3Qtz = 2Or_{Kfs} + Py_{Grt} + 2H_2O. \quad (10)$$

Notable is the retrograde shift of bulk composition in reacting domains towards higher Mg contents than the original bulk-rock composition, because Fe-rich garnet cores become isolated. Garnet rim composition becomes more magnesian in contact with Fe–Mg phases such as phengite and newly formed biotite, indicating the direction of crossing of Fe–Mg exchange reactions after the *PT* maximum.

GEOTHERMOBAROMETRY AND FLUID EVOLUTION

Methods

The *PT* conditions of metamorphism were estimated primarily by calculation of multivariant equilibria between mineral components using the internally consistent

thermodynamic data set of Berman (1988; updated in 1992) and applying the Ge0-Calc software of Brown *et al.* (1988) to yield consistent data. The data set was in particular augmented by the compatible data for the mineral component Al-celadonite as derived by Massonne (1991, 1995). The following nonideal activity models were used for solid solutions: garnet (Berman, 1990), biotite (McMullin *et al.*, 1991), plagioclase and K-feldspar (Fuhrman & Lindsley, 1988), and phengite (Massonne, 1995). The thermodynamic data for Al-celadonite and the activity models for phengite (Massonne, 1995) are based on experimental data summarized by Massonne (1991). Ideal activity models were adopted for sphene and ilmenite, whereas the activities of kyanite, rutile and quartz were set to unity.

Biotite was not used in calculation of the maximum *PT* conditions, because it can be shown that this phase was, in most cases, not stable at these conditions. Generally the cores of garnet, plagioclase and white mica were correlated for the earliest recognizable equilibration stage. The water-independent equilibria (3), (4) and (5) were used as barometers. GASP barometry [reaction (3)] was found to be in good agreement with the calibration of Koziol & Newton (1988). The only reliable thermometer for the early equilibration stage was the two-feldspar thermometer. Exsolution lamellae in relic cores of large plagioclase and potassic feldspar grains in assemblages 1 and 2 were reintegrated using back-scattered electron (BSE) images as well as analyses with a wide electron beam. The reconstituted feldspar compositions (Fig. 2; Table 3) were used to derive temperatures by the two-feldspar thermometer of Fuhrman & Lindsley (1988), adapting both compositions to a ternary solvus (Kroll *et al.*, 1993). Finally, water-dependent reactions involving K-feldspar were calculated to estimate water activities at independently derived peak *PT* conditions. Together with reactions (1) and (2), these are, for stage I,

$$\mathrm{Grs_{Grt}} + 2\mathrm{Ms_{WM}} + 3\mathrm{Qtz} = 3\mathrm{An_{Pl}} + 2\mathrm{Or_{Kfs}} + 2\mathrm{H_2O} \quad (11)$$

$$3\mathrm{An_{Pl}} + 6\mathrm{Ace_{WM}} = \mathrm{Grs_{Grt}} + 6\mathrm{Or_{Kfs}} + 2\mathrm{Py_{Grt}} + 3\mathrm{Qtz} + 6\mathrm{H_2O}. \quad (12)$$

For retrograde re-equilibration in local rock domains (stage II), biotite compositions were used in conjunction with

$$\mathrm{Alm_{Grt}} + 3\mathrm{Ace_{WM}} = \mathrm{Ann_{Bt}} + \mathrm{Ms_{WM}} + \mathrm{Phl_{Bt}} + \mathrm{Qtz} \quad (13)$$

$$\mathrm{Py_{Grt}} + 3\mathrm{Ace_{WM}} = \mathrm{Ms_{WM}} + 2\mathrm{Phl_{Bt}} + 6\mathrm{Qtz} \quad (14)$$

$$\mathrm{Alm_{Grt}} + \mathrm{Phl_{Bt}} = \mathrm{Py_{Grt}} + \mathrm{Ann_{Bt}} \quad (15)$$

$$2\mathrm{Alm_{Grt}} + 3\mathrm{Ace_{WM}} = 6\mathrm{Qtz} + \mathrm{Py_{Grt}} + \mathrm{Ms_{WM}} + 2\mathrm{Ann_{Bt}}. \quad (16)$$

The Fe–Mg exchange reaction between garnet and biotite, as calculated in this study, yielded temperatures up to 50°C higher than conventional thermometers including good Ca corrections for garnet (Hodges & Spear, 1982; Ganguly & Saxena, 1984).

In assemblage 3, the following reactions may also be used for *PT* calculations using Ti-bearing phases:

$$\mathrm{Alm_{Grt}} + 3\mathrm{Rt} = 2\mathrm{Qtz} + \mathrm{Ky} + 3\mathrm{Ilm} \quad (17)$$

$$2\mathrm{Alm_{Grt}} + \mathrm{Phl_{Bt}} + 6\mathrm{Rt} = 3\mathrm{Qtz} + \mathrm{Py_{Grt}} + \mathrm{Ms_{WM}} + 6\mathrm{Ilm} \quad (18)$$

$$\mathrm{Alm_{Grt}} + \mathrm{Ann_{Bt}} + 6\mathrm{Rt} = 3\mathrm{Qtz} + \mathrm{Ms_{WM}} + 6\mathrm{Ilm}. \quad (19)$$

Water-dependent reactions involving K-feldspar were again used for hygrometric estimates of the retrograde stage II:

$$\mathrm{Ann_{Bt}} + \mathrm{Ms_{WM}} + 3\mathrm{Qtz} = 3\mathrm{Alm_{Grt}} + 2\mathrm{Or_{Kfs}} + 2\mathrm{H_2O} \quad (20)$$

$$\mathrm{Ms_{WM}} + 3\mathrm{Ace_{WM}} = 4\mathrm{Or_{Kfs}} + \mathrm{Py_{Grt}} + 4\mathrm{H_2O} \quad (21)$$

$$\mathrm{Alm_{Grt}} + 3\mathrm{Ace_{WM}} = \mathrm{Ann_{Bt}} + 2\mathrm{Or_{Kfs}} + \mathrm{Py_{Grt}} + 3\mathrm{Qtz} + 2\mathrm{H_2O} \quad (22)$$

$$3\mathrm{Ace_{WM}} = \mathrm{Phl_{Bt}} + 2\mathrm{Or_{Kfs}} + 3\mathrm{Qtz} + 2\mathrm{H_2O}. \quad (23)$$

For *PT* estimation of early retrograde equilibration in the single pyroxene–garnet symplectite found in assemblage 1, the conventional Fe–Mg exchange thermometer as calibrated by Ellis & Green (1979) was applied, and for pressure estimation the clinopyroxene–plagioclase–quartz barometer of Gasparik & Lindsley (1980) was used.

White mica may coexist with rutile and quartz during the prograde *PT* path, at peak conditions and during the retrogade *PT* path in all assemblages, thus providing an excellent opportunity to apply the Ti-muscovite–rutile–quartz barometry of Massonne *et al.* (1993). This method requires only the coexistence of rutile, white mica and quartz. This empirically calibrated barometer is based on the following multivariant reaction and uses a nonideal activity model for white mica:

$$\mathrm{Ms_{WM}} + 2\mathrm{Rt} = \mathrm{Ti\text{-}Ms_{WM}} + 2\mathrm{Qtz} \quad [\mathrm{Ti\text{-}Ms} = \mathrm{KAl_3Ti_2SiO_{10}(OH)_2}]. \quad (24)$$

RESULTS AND DISCUSSION

Assemblage 1

Consistent temperatures of 830°C were derived by two-feldspar thermometry for four samples from di erent localities (A in Fig. 13) using reintegrated core compositions of coexisting plagioclase and K-feldspar with preserved exsolution lamellae. The assumed pressure of 22–23 kbar was derived by GASP barometry [reaction

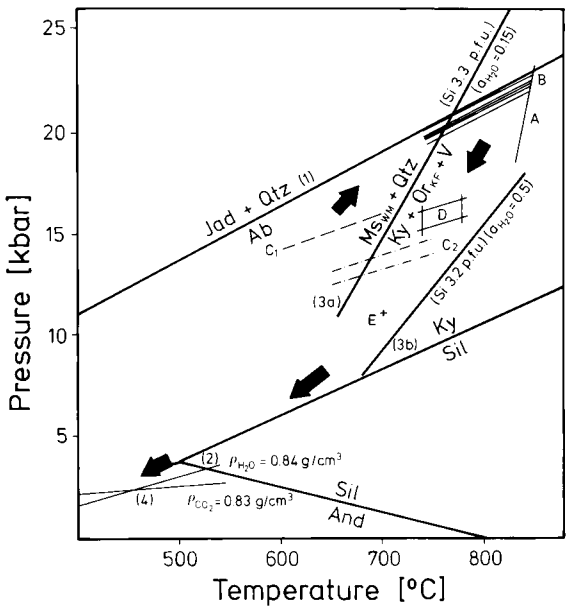

Fig. 13. *PT* history for rocks of assemblage 1 (kyanite granulites). (For a discussion of equilibria A–E, see text.) 1, Holland (1980); 2, aluminosilicate stability field after Holdaway (1971); 3, reactions calculated with the modified thermodynamic data set of Berman (1988); 4, isochores of mean compositions of secondary fluid inclusions [Krentz *et al.*, 1990; Thomas, personal communication to Rötzler (1995)].

(3); equilibrium B in Fig. 13] with core compositions of garnet and plagioclase. Inclusions of phengite and paragonite in garnet, kyanite and zircon point to a lower-temperature equilibration event before trapping. Plagioclase inclusions are generally albite as in the matrix, but enclosed oligoclase was also found. This also points to lower pressures before trapping in an assumed prograde assemblage with garnet, quartz and kyanite. Independent proof is provided by Ti-muscovite barometry of phengite enclosed together with rutile in zircon (C1 in Fig. 13). It was this particular zircon which was dated by Kröner & Willner (1995) with the Pb–Pb evaporation method, yielding 340 Ma as the age of metamorphic zircon growth during the prograde path approaching the thermal peak at elevated pressures. No later modification of the inclusion composition appears to have occurred, as is also supported by the lack of cracks propagating towards these inclusions, or any sign of exchange with the host mineral. Hence garnet as well as kyanite and zircon grew on the late prograde path close to the pressure maximum. However, garnet core composition can be expected to have homogenized at the very high peak temperatures of >800°C by volume di usion and thus should not be used to calculate prograde *PT* conditions.

Very small quartz–K-feldspar–plagioclase and quartz–K-feldspar aggregates enclosed in garnets, as well as irregular granitic veins lacking biotite or white mica may be interpreted as relics of dehydration melts. This suggests that the breakdown of biotite and white mica may in part have involved melt-producing reactions such as

$$\text{Bt} + \text{WM} + \text{Plag} + \text{Qtz} = \text{Grt} + \text{Kfs} + \text{L}. \quad (25)$$

At the maximum *PT* conditions considered here dehydration melts were produced experimentally by Le-Breton & Thompson (1988) by the breakdown of biotite with intermediate Fe/Mg ratios. Such melts could have absorbed additional water, one of the possible reasons for the strong reduction of water activity in these rocks (see below).

Because maximum *PT* conditions are close to the upper stability field of albite, the question arises as to whether the jadeite stability field was ever crossed. No jadeite was trapped in any phase, although even earlier, lower-pressure prograde phases are present. If the rocks were ever subjected to the conditions of the jadeite stability field, the formation of jadeite must have been prevented for kinetic reasons.

The early retrograde formation of omphacite–plagioclase symplectites observed in one sample occurred at 745–780°C and 15–17 kbar, according to clinopyroxene–garnet thermometry (using garnet core compositions) and clinopyroxene–plagioclase–quartz barometry (field D in Fig. 13). The spread of omphacite composition is reflected by the range of *PT* data. The conditions of formation of retrograde white mica were estimated for two samples by Ti-muscovite barometry as 12–13 kbar at assumed temperatures of 700°C (curves C_2 in Fig. 13). A further retrograde *PT* coordinate at 11 kbar and 695°C was estimated in one sample from reactions (3) and (14), using rim compositions of garnet 1 and plagioclase in contact (E in Fig. 13). Barometry using rim compositions of plagioclase is di cult and hazardous owing to widely variable rim compositions. On the basis of the available data, the retrograde *PT* path must have involved an initial strong decompression of >10 kbar, accompanied by cooling of <100°C (see Fig. 13).

The calculated positions of the white mica + quartz breakdown curves [reaction (1)] suggest that water activities must have been below 0·15 at peak *PT* conditions (white mica unstable), increasing to at least 0·5 during retrograde formation of white mica. This early retrograde increase in water activity must reflect external hydrous fluid influx responsible for the growth of mica.

No alteration of kyanite to sillimanite or growth of sillimanite by any other reaction has ever been observed in the Central Erzgebirge. Hence it is suggested that the late retrograde *PT* path might generally have been restricted to the kyanite stability field. As in all other rocks of the Central Erzgebirge, late secondary fluid inclusions were trapped at low pressures (Krentz *et al.*,

1990; Thomas, personal communication to Rötzler, 1995). Typical isochores for mean secondary hydrous and CO_2-rich fluid inclusions are shown in Fig. 13, suggesting that the rocks were below 3 kbar after crossing the 500°C isotherm, where greenschist-facies minerals such as chlorite, epidote and fine-grained white mica were formed, particularly in rocks deformed by the D_3 phase.

Assemblage 2 and metablastic gneisses

Here also the only reliable estimates of maximum temperature conditions are provided by two-feldspar thermometry, using relic integrated core compositions of coexisting plagioclase and K-feldspar. However, such relics are rare in assemblage 2; only in sample E29e could a temperature of 780°C be calculated for 20 kbar (A in Fig. 14). Such maximum pressures of 18–21 kbar may be derived by calculating the multivariant reaction (4), using core compositions of garnet, plagioclase and phengite (B in Fig. 14). These show little variation in each sample; moreover, the core compositions of matrix plagioclase and phengite are similar to those enclosed in garnet. Somewhat lower pressures of 17–18·5 kbar were calculated independently for the same phengites by Ti-muscovite barometry (D in Fig. 14). Calculated reactions involving sphene and rutile in sample E29e intersect reaction (4) at 760°C and 21 kbar (C in Fig. 14). These maximum *PT* conditions near the upper stability limit of albite are comparable with those found for assemblage 1. Again, all geothermobarometry depends on the existence and stability of plagioclase, which is also an abundant inclusion phase in garnet. These rocks show no sign that they were ever subjected to conditions of the jadeite stability field. Owing to the stronger retrograde overprint, it is hazardous to attempt derivation of maximum *PT* conditions for the widespread metablastic gneisses in a similar way.

For three samples of assemblage 2, water activities were calculated with the water-dependent reactions (2), (11) and (12). The estimated values of 0·15–0·4 well exceed those suggested for assemblage 1. Hence the existence of phengite in the presence of quartz at peak metamorphic conditions definitely depends on a higher water activity in these rocks.

Calculating early retrograde equilibria is di cult owing to the existence of two garnet generations and strongly variable compositions of plagioclase rims and biotite. However, in the overprinted metablastic gneisses a more restricted compositional variation in biotite indicates better re-equilibration. Multivariant reactions (13)–(16) were calculated for garnet and phengite rim compositions in contact with biotite, including pairs from overprinted gneiss samples as well. *PT* coordinates scatter strongly at

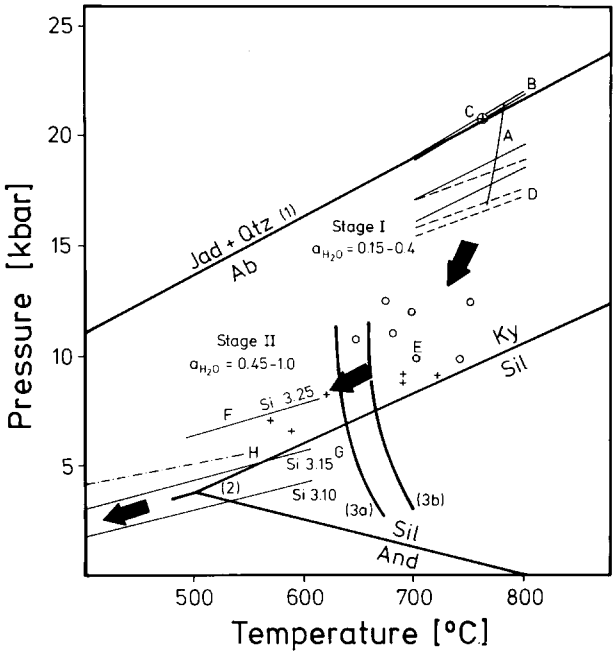

Fig. 14. *PT* history for rocks of assemblage 2. (For discussion of equilibria A–H, see text.) 1, Holland (1980); 2, aluminosilicate stability field after Holdaway (1971); 3a, wet granite solidus, 3b, wet tonalite solidus according to Johannes (1984).

580–750°C and 6–12 kbar (see symbols labelled E in Fig. 14). There is a tendency toward higher *PT* values for garnet 1 rims (circles for E in Fig. 14) as compared with those calculated from garnet 2 rims (crosses for E of Fig. 14). The water-dependent reactions (19)–(22) involving K-feldspar were calculated for hygrometric estimates at the *PT* values obtained. As in assemblage 1, a strong relative increase in water activities to values ranging between 0·45 and 1·0 is an obvious indication of water addition during retrograde biotite growth.

An independent corroboration of the second equilibration stage is given by migmatitic gneisses. Average Si contents of white micas in partial melts of tonalitic and granitic composition are 3·25 p.f.u. [F in Fig. 14; isopleth after Massonne (1991)], indicating a pressure of 8–9 kbar at the intersection with the wet granite and tonalite solidi. Conditions of 616–688°C and 8–8·5 kbar with $a_{H_2O} = 0{\cdot}8–1{\cdot}0$ may be calculated for the migmatitic gneiss E43e with granitoid composition, using multivariant equilibria. Hence widespread anatexis in metablastic gneisses is a retrograde phenomenon strongly related to abundant hydration.

Barometry with reactions involving the anorthite component of plagioclase gives only pressures in the detected range for the formation of garnet 2, when the rare rim compositions of plagioclase with the highest An contents are considered. This indicates that grossular-rich garnet 2 was in equilibrium with local late oligoclase.

The data again indicate early decompression of up to 10 kbar and subsequent cooling within the kyanite stability field. Later retrograde re-equilibration occurred, especially where discrete, ductile s_3 shear zones deform the rocks. Some recrystallized feldspars indicate that deformation already occurred above the 500°C isotherm. Ti-muscovite barometry of the recrystallized low-Si white micas (H in Fig. 14), as well as the respective Si isopleth for assemblages with biotite and K-feldspar (G in Fig. 14), indicate that the rocks had attained pressures of 2·5–4 kbar after cooling to ~400–500°C.

Assemblages 3a and 3b

In these rocks, the number and chemical variation of phases in both metapelitic assemblages without K-feldspar is fairly restricted, in particular for a treatment with conventional geothermobarometry. On the other hand, Ti-muscovite barometry may be applied extensively. Using core compositions of matrix phengites and phengite inclusions in garnet, a wide pressure range between 12 and 24 kbar at an assumed maximum 700–800°C results (dashed curves B in Fig. 15), whereby the inclusion phengites consistently yield higher pressures in all samples (curves A in Fig. 15). In Fig. 15 somewhat lower temperatures are assumed during equilibration of the inclusion phengites relative to the first equilibration of the matrix phengites in accordance to the observations made with the other assemblages. The following major conclusions may be extracted from these relationships and should also be applicable to all other rocks of the Gneiss–Eclogite Unit.

A large difference in the maximum pressures attained seems to exist between different rocks of the Gneiss–Eclogite Unit. Some acid rocks of the Gneiss–Eclogite Unit may in fact even have equilibrated in the jadeite stability field. Hence the quartzo-feldspathic rocks of the unit delineate a metamorphic array rather than a unique *PT* path at maximum pressures. The remarkable pressure differences consistently indicated by core compositions of the matrix phengites and of the inclusion phengites for different samples are independently corroborated by the evident differences in the Si contents of the white micas. These presumably record pressure differences, because they mostly occur in a limiting assemblage with garnet, kyanite and quartz. The resulting multivariant barometer reaction (see Fig. 10)

$$\mathrm{Ace_{WM}} + \mathrm{Ky} = \mathrm{Ms_{WM}} + \mathrm{Py_{Grt}} + \mathrm{Qtz} \qquad (26)$$

is also water independent (however, owing to the very low activities of pyrope in garnet this reaction was not used for barometry). There is no recognizable regional trend in the distribution of these calculated maximum pressures, because the tectonic position of the samples is rather difficult to correlate from outcrop to outcrop. However, if the different white mica compositions were actually an effect of differential preservation during uplift and variable diffusion kinetics at high temperatures, then the consistently similar trend between matrix and inclusion white micas should not be seen. White micas are rather large in rocks with assemblage 3, and diffusion of Al, Si or Ti would involve complex substitutions and, hence, would also be rather slow. Furthermore, retrograde reaction to biotite is very limited in these rocks.

Retrograde *PT* data, including the growth of biotite in assemblages 3a and 3b, fall into the same range as for all other gneisses: *PT* coordinate C in Fig. 15 was calculated in the same way as for assemblage 2 in Fig. 14, whereas point D was derived by calculation of equilibria (17), (18) and (19) with rutile and ilmenite.

The calculation of water-dependent reaction (2) with average mineral compositions of an assemblage including phengite with Si = 3·3 p.f.u. and a theoretical K-feldspar (curve 3 in Fig. 15) indicates that water activities have generally exceeded 0·4 in all rocks of assemblage 3 at maximum *PT* conditions and during decompression.

Hence those assemblages lacking K-feldspar were in fact the most hydrous assemblages during maximum *PT* conditions among the rocks studied. Kyanite was never found altered to sillimanite in rocks of paragenesis 3a within the entire unit, again indicating that most probably the entire retrograde *PT* path lay within the kyanite stability field.

CONCLUSIONS

Most quartzo-feldspathic and metapelitic rocks of the Gneiss–Eclogite Unit in the Central Erzgebirge were subjected to HP–HT metamorphism leading to ubiquitous prograde biotite breakdown and the formation of grossular-rich garnet in granitoid rock compositions in the uppermost stability field of albite, with phengite in part stable and in part absent in the presence of quartz. Thus metamorphism under maximum *PT* conditions occurred within the extremely wide transitional field of the granulite, eclogite and amphibolite facies. The lower limit of stability of such Ca-rich garnets in albite-bearing rocks of granitic composition is probably ~10–12 kbar at 700°C, as such maximum conditions prevailed in the underlying Red and Grey Gneiss Unit where granitoid orthogneisses mostly lack garnet (Klemm, 1995; Rötzler, 1995; Kröner *et al.*, 1995). Separation of the pressure and temperature maximum—where at all possible—was minor, indicating no major thermal relaxation after the pressure peak, i.e. exhumation and cooling were sufficiently rapid to prevent the temperature increase that

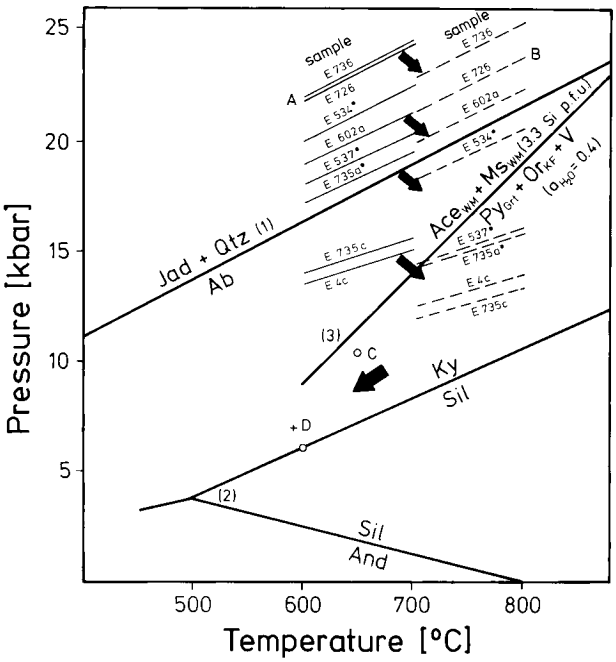

Fig. 15. *PT* history for rocks of assemblages 3a and 3b. (For a discussion of equilibria A–D, see text.) 1, Holland (1980); 2, aluminosilicate stability field after Holdaway (1971); 3, reaction calculated with the modified thermodynamic data set of Berman (1988), using average garnet and white mica compositions.

would have occurred during any delay near maximum metamorphic conditions.

Variable water activity governed the stability of three di erent, predominantly biotite-free acid assemblages at peak metamorphic conditions. Kyanite granulites, which may be completely devoid of any hydrous phase (particularly phengite), are the rocks with the lowest water activity (<0·15), followed by rocks with phengite stable together with quartz, garnet, plagioclase and K-feldspar. These indicate intermediate water activities (0·15–0·4). Metapelitic rocks without K-feldspar but with stable phengite must have had water activities well exceeding 0·4. This means that water activity was strongly reduced only in some rocks, and variable in most others at peak metamorphic conditions. Preservation of such short-range di erences in a penetratively extremely deformed rock unit with subsequent fluid influx is good evidence that later retrograde fluid flow was strongly channelized.

Variable availability of water must have had a strong influence on the preservation of relic deformation features such as the HT mylonite fabric. Preservation of this fabric was only possible owing to (1) strong reduction of prevailing water activity after formation and (2) short duration of high temperatures. The deformation responsible for the penetrative s_2 foliation of the Gneiss–Eclogite Unit may be directly observed in this preserved relic HT mylonitic fabric and occurred after formation of the peak assemblage, because all maximum *PT* phases can show signs of this deformation. By contrast, retrograde biotite in the HT mylonites is always undeformed, indicating that the D_2 deformation, characterized by extreme flattening, is associated with the strong, near-isothermal decompression that followed the equilibration stage at maximum *PT*. This is interpreted as large-scale, deep-seated stretching within overthickened crust during an early retrograde extensional event. Tectonic transport was in an east–west direction, as indicated by the consistent direction of the stretching lineation in the entire unit.

During this event, rocks representing di erent depths of burial must have been brought together. The maximum pressures of garnet peridotites and most eclogites well exceed those of most acid rocks. Even the maximum pressures within the metapelitic gneisses were shown to di er by up to 8–10 kbar.

Retrograde biotite growth is observed in all rocks to a highly variable degree at intermediate pressures and temperatures between 600 and 750°C. Estimated water activities increased to 0·4–1·0 during this stage. Retrograde formation of tonalitic and granitic partial melts is observed in widespread migmatitic gneisses at the wet solidus. Such features imply pronounced external fluid influx at this stage during uplift. However, fluid flow was strongly channelized, as indicated by the extreme variability of overprint within these rocks. Willner (1994) has shown that the local presence of Cl-rich biotites

within rocks of the Gneiss–Eclogite Unit indicates the preservation of locally reduced water activities. This must be a sign of localized fluid flow, because any low fluid influx would be su cient to homogenize Cl activity gradients.

The strong zoning observed in all phases is normally an unexpected feature in HT rocks. The strong decrease in Fe/(Fe + Mg) of garnet in contact with Fe–Mg phases such as phengite and biotite, along with the marked decrease in garnet grossular component in all rocks studied, is consistent with a distinctive decompression path that is steeper in dP/dT slope than the curves of constant Fe–Mg fractionation for Fe–Mg exchange reactions. The same e ect is prominent in biotites from rocks still preserving evidence of low water activity (Fig. 9), in which the corresponding increase in Fe/(Fe + Mg) is combined with decreasing Si on the order of 0·2 p.f.u. Massonne (1991) has shown that such a decrease of Si in pure phlogopite in the presence of phengite, K-feldspar and quartz could correspond to an ~10 kbar in isothermal pressure release.

Late reversal rims in garnet, in which Fe/(Fe + Mg) once again increases, reflect predominant cooling until a critical closing temperature for volume di usion was reached. These rims are very narrow and indicate that cooling after the initial near-isothermal decompression was very rapid. Thus the observed zoning in garnet is a feature largely due to di usion at very high temperatures that was frozen-in because of later rapid cooling rates. The restriction of late retrograde re-equilibration to local rock domains is a further corroboration of this conclusion.

A particularly puzzling phenomenon, intimately connected with retrograde fluid infiltration, is the growth of a second grossular-enriched garnet generation after grossular decrease and garnet resorption of the first generation. The possibility of a further strong increase in pressure after an initial decompression must be rejected owing to (1) the lack of analogous zonation features in all other phases, (2) the lack of evidence for a second decompression and resulting resorption phenomena in second-generation garnet, and (3) the proven local equilibration between the rims of coexisting phases and the very Ca-rich plagioclase rims after the major first decompression of the rocks at transient medium-pressure conditions. External influx of Ca-rich hydrous fluids on a rather local scale may be proposed to explain Ca enrichment in the garnet rims of plagioclase-free and hence Ca-poor assemblage 3a, where Ca-richer fluids would come from surrounding plagioclase-bearing rocks. However, it would be an improbable explanation for garnet 2 growth in the most abundant plagioclase-bearing rocks, because there is no evidence for a possible source of Ca-richer fluids on a regional scale.

As a third possibility, formation of the second grossular-rich garnet might be due to (1) kinetic control of the di erential rate of material availability for the growth of new minerals, while the first garnet was resorbed during isothermal decompression, and (2) garnet growth during subsequent rapid cooling in a markedly changed local domain bulk composition. It is obvious that only a small volume of the existing albite reacted at the outermost rims, and volume di usion within the albite grains was extremely slow. Thus only a very restricted amount of albite in the rock was available for the retrograde reaction to oligoclase. In contrast, breakdown of the Fe–Mg components in garnet to form new biotite would have taken place readily at appropriate conditions after pressure release and increase in water availability. This would also have favoured very rapid dissolution of the unstable grossular component. The combination with the concomitant retarded formation of more An-rich plagioclase should have led to a transient enrichment of Ca in the fluid phase and hence to a transient Ca-rich environment in local domains of the rock. During rapid cooling after decompression grossular-forming reactions would be cut with a flat angle. Locally therefore, a new stable grossular-rich garnet grew again in local equilibrium with a high Ca-plagioclase showing also local equilibration with biotite and phengite in the range 720–570°C and 6–8 kbar (Fig. 13).

In summary, the early stage of uplift and retrograde *PT* evolution can be characterized as follows:

(1) A HP–HT equilibration event in a region of low geothermal gradient was followed by a near-isothermal decompression of as much as 10 kbar with a minor temperature decrease of <100°C.

(2) The formation of the prominent penetrative s_2 foliation is bracketed by the above HP–HT event and medium-pressure retrograde equilibration with external fluid influx. A strong stretching of the crust occurred as well as a juxtaposition of rocks subjected to di erent maximum, but invariably high pressures. Hence the entire rock pile represents a major extensional shear zone in the lower part of continental crust with excess crustal thickness. Very di erent levels of this lower crust were amagalmated during the D_2 deformation. The process ended with a major influx of hydrous fluids at medium-pressure conditions, leading to pronounced, but variable, re-equilibration.

(3) The uplift at high temperatures must have been very rapid, because (a) strong mineral zoning during HT decompression is mostly still preserved, (b) HT deformation fabrics are locally preserved in dry rocks and (c) no major thermal relaxation, i.e. temperature increase, occurred after the pressure maximum.

(4) The second part of the *PT* path monitoring the final exhumation of the Gneiss–Eclogite Unit has a di erent geometry and is characterized by less pronounced pressure release and extensive cooling. Discrete ductile shear zones with normal fault kinematics radial

to the pronounced dome structures (Fig. 1; Krohe, 1997) developed during cooling to below the 500°C isotherm at 2·5–4 kbar pressure, as indicated by recrystallized low-Si white micas and secondary fluid inclusions. There are no signs that this late *PT* evolution ever took place outside the kyanite stability field, in contrast to the retrograde evolution of HP granulites in the nearby Granulite Massif (Rötzler, 1992) or Lower Austria (Carswell & O'Brien, 1993). Very narrow retrograde re-equilibration rims in garnet are due to cooling and indicate a rapid transition from high temperatures near 700°C to closing temperatures of 550–600°C for di usion processes in garnet. Although both markedly di erent branches of the *PT* path indicate di erent confining conditions, it is unlikely that there was a long time gap between these two episodes.

CONSTRAINTS FOR VARISCAN GEODYNAMICS

This publication contributes to the understanding of a rather specific group of granulites that are widespread along the Variscan chain of Europe from Spain to Poland, the so-called 'group I granulites' of Vielzeuf & Pin (1989). These restricted and scattered occurrences are strikingly similar, although from widely separated areas of the continent. GASP barometry in kyanite granulites yields maximum pressures ranging from 13 to 20 kbar. Associated with these felsic HP granulites are mafic granulites, garnet peridotites and/or eclogites. A retrograde amphibolite facies overprint producing dominant migmatitic gneisses is observed, but a later HT–LP overprint is generally lacking. In particular, many group I granulite units are known surrounding the Bohemian Massif [see review by O'Brien & Carswell (1993)], where *PT* evolutions comparable with those in the Central Erzgebirge were derived, e.g. in the Polish Sudetes (Sowie Gory: O'Brien *et al.*, 1996; Snieznik: Steltenpohl *et al.*, 1993; Kryza *et al.*, 1996), the Saxonian Granulite Massif (Rötzler, 1992) or in Lower Austria (Carswell & O'Brien, 1993). Although this type of metamorphism was regarded as mainly Early Variscan in Western Europe by Vielzeuf & Pin (1989), the age of the metamorphic peak in the Central European occurrences seems to range from early Devonian to early Carboniferous, e.g. 400 Ma in Sowie Gory (O'Brien *et al.*, 1996) and 340 Ma in the Saxonian Granulite Massif (Von Quadt, 1993). Because high-pressure granulites seem to be rare world-wide, according to the review by Harley (1989), HP granulitic rocks must be of special importance in the evolution of the Hercynian belt, indicating a widespread specific geotectonic environment (O'Brien & Carswell, 1993).

As in the above occurrences, maximum peak *PT* conditions in the Gneiss–Eclogite Unit were dated at 340 Ma (Kröner & Willner, 1995; Kotková *et al.*, 1996; Willner *et al.*, 1996; $^{207}Pb/^{206}Pb$ ages of metamorphic zircons). Similar ages of 333–360 Ma (Sm–Nd mineral–whole-rock isochrons) and 348–355 Ma (Ar–Ar plateau ages for phengites) were provided by Schmädicke *et al.* (1995), dating eclogites of the Gneiss–Eclogite Unit. Abundant Ar–Ar plateau ages of white micas and hornblende consistently range around 338 Ma in the Gneiss–Eclogite Unit, as in the units below and above, similar to Rb/Sr ages of white micas (Werner *et al.*, 1996). This overlap derived from isotopic systems with di erent closure temperatures requires extremely fast tectonic exhumation. Exhumation must have been terminated by 325 Ma at the latest, as shown by the first regional unconformity (Kurze, 1966). Hence all processes related to exhumation occurred during the peak of the Variscan orogeny and were very rapid, favouring tectonic thinning at rates on the order of those proposed by England & Thompson (1986). The high maximum pressures recorded indicate derivation of the quartzo-feldspathic rocks from the lower part of a crust thickened to >60 km along a geothermal gradient slightly exceeding 10°C/km, thus somewhat higher than commonly inferred for typical subduction metamorphism in accretionary prisms. From the age constraints, exhumation rates of at least 4 mm/yr result.

The preserved pressure–temperature–deformation evolution is a history of continuous retrograde extension responsible for exhumation. The same *PT* path, with its characteristic geometry, was also recognized by Kotková (1993) for granulites on the Czech side of the Erzgebirge, also indicating that the typical conditions prevailing in the Gneiss–Eclogite Unit were similar over a regional extent. A comparable *PT* path was also detected in the HP granulites of Lower Austria, indicating widespread similar geotectonic conditions (Carswell & O'Brien, 1993).

HP metamorphism is commonly masked by an amphibolite-facies overprint, but fortunately, except for the easternmost Erzgebirge, not by the HT–LP metamorphism typical for the Moldanubian region further south. Hydrous fluid influx leading to a general increase of water activity and finally to abundant retrograde anatexis at the wet solidus in the most overprinted gneisses cannot solely be produced by dehydration reactions during decompression (mostly involving breakdown of the Al-celadonite component), as proposed, for instance, by Heinrich (1982) for HP metapelites in the vicinity of eclogites. Although some reactions of this type certainly occur, as shown above, there should at least be a retrograde reduction of water activity in many acid rocks. However, changes in water activity could not be recorded in the K-feldspar-free assemblages, and the 'driest' conditions invariably occurred at peak metamorphic conditions in all K-feldspar-bearing rocks. On the other hand, if the HP unit were thrust onto another crustal unit

undergoing prograde dehydration during uplift, another source for hydrous fluid influx would be provided.

Continued crustal stacking must, in fact, be expected, to exhume rocks from the lower part of an overthickened crust to the surface in a single orogenic cycle. By pure extension of the entire crust only, such rocks would remain in the lower part of a normal isostatically equilibrated crust (Ellis, 1987). In the case of the Central Erzgebirge, it was shown by Rötzler (1995) and Klemm (1995) that the underlying Red and Grey Gneiss Unit was subjected to intermediate maximum pressures only, and also to lower peak temperatures. Such tectonic insertion of the HP–HT unit into intermediate crustal levels would also provide the possibility of more rapid cooling during further uplift, as indicated by the second branch of the retrograde *PT* path of the Gneiss–Eclogite Unit. Towards the overlying Mica-Schist–Eclogite Unit there is also a marked '*PT* discontinuity' to much lower peak conditions (Rötzler, 1995). Hence, during decompression from medium-pressure to low-pressure conditions (second branch of the *PT* path), the entire HP–HT unit was probably cooled from below and above.

Therefore the overall position of the entire HP–HT Gneiss–Eclogite Unit is one of a dismembered subhorizontal nappe unit sandwiched between other crustal units of contrasting *PT* evolution by ductile deformation processes occurring during uplift into mid-crustal levels, but definitely not at a coherent regional suture zone. Also, the Erzgebirge crystalline complex cannot be the basement for the neighbouring Saxothuringian basin with unmetamorphosed to low-grade sediments, because sedimentation was still continuing in the basin when HP metamorphism occurred in the crystalline complex. Juxtaposition of these contrasting terranes can be explained by large-scale movements with lateral components during uplift of the crystalline complex, in particular when rocks were still within the ductile deformational regime (Krohe, 1997).

The processes deduced from the Gneiss–Eclogite Unit, which obviously occurred in similar widespread areas within Central Europe, point to a prolonged period of crustal stacking and crustal thickening of vast volumes of continental crust, followed by very rapid exhumation of HP slices from the lower part of the thickened crust. Such features are of continental extent and must be due to continuous continent–continent collision during the Variscan orogeny, rather than subduction at a convergent plate margin before continent–continent collision.

ACKNOWLEDGEMENTS

This research project was supported by grants of the Deutsche Forschungsgemeinschaft (Ma 689/6 and Ma 689/10), which are gratefully acknowledged. The paper is also a contribution to the DFG priority programme 'Orogenic processes with particular reference to the Variscides'. J. Kopp is thanked for first introduction to the field, initiation of the project and support in numerous other ways. Careful reviews by G. T. R. Droop and P. J. O'Brien substantially improved the manuscript.

REFERENCES

Behr, H. J., Fritsch, E. & Mansfeld, L., 1965. Die Granulite von Zöblitz im Erzgebirge als Beispiel für Granulitbildung in tiefreichenden Scherzonen. *Krystallinikum* **3**, 7–29.

Bergner, R., 1990. Vergleichende Untersuchungen an temperaturbetont metamorphisierten Gesteinen ausgewählter Einheiten des Saxothuringikums. *Freiberger Forschungshefte* **C434**, 6–66.

Berman, R. G., 1988. Internally-consistent thermodynamic data for minerals in the system Na_2O–K_2O–CaO–MgO–FeO–Fe_2O_3–Al_2O_3–SiO_2–TiO_2–H_2O–CO_2. *Journal of Petrology* **29**, 445–522.

Berman, R. G., 1990. Mixing properties of Ca–Mg–Fe–Mn garnets. *American Mineralogist* **75**, 328–344.

Bernhardt, H. J., Massonne, H.-J., Reinecke, T., Reinhardt, J. & Willner, A. P., 1995. Digital element distribution maps, an aid for petrological investigations. *Berichte der Deutschen Mineralogischen Gesellschaft, Beiheft 1 zum European Journal of Mineralogy* **7**, 28.

Brown, T. H., Berman, R. G. & Perkins, E. H., 1988. Ge0-Calc: Software package for calculation and display of pressure–temperature–composition phase diagrams using an IBM or compatible personal computer. *Computers and Geoscience* **14**, 279–289.

Carswell, D. A. & O'Brien, P. J., 1993. Thermobarometry and geotectonic significance of high-pressure granulites: examples from the Moldanubian zone of the Bohemian Massif in Lower Austria. *Journal of Petrology* **34**, 427–459.

Ellis, D. J., 1987. Origin and evolution of granulites in normal and thickened crust. *Geology* **15**, 167–170.

Ellis, D. J. & Green, D. H., 1979. An experimental study of the e ect of Ca upon garnet–clinopyroxene Fe–Mg-exchange equilibria. *Contributions to Mineralogy and Petrology* **71**, 13–21.

England, P. C. & Thompson, A. B., 1986. Some thermal and tectonic models for crustal melting in continental collision zones. In: Coward, M. P. & Ries, A. C. (eds) Collision Tectonics. *Geological Society of London, Special Publication* **19**, 83–94.

Freyer, G., Hoth, K. & Sehnert, M., 1994. Kenntnisstand bis 1990/91 über die Fossilführung im Bereich des Erzgebirges. *Zeitschrift für geologische Wissenschaften* **22**, 555–565.

Fuhrman, M. L. & Lindsley, D. H., 1988. Ternary feldspar modeling and thermometry. *American Mineralogist* **73**, 201–215.

Ganguly, J. & Saxena, S. K., 1984. Mixing properties of aluminosilicate garnets: constraints from natural and experimental data, and applications to geothermobarometry. *American Mineralogist* **69**, 88–97.

Gasparik, T. & Lindsley, D. H., 1980. Phase equilibria at high pressure of pyroxenes containing monovalent and trivalent ions. In: Prewitt, C. T. (ed.) Pyroxenes. *Reviews in Mineralogy, Mineralogical Society of America* **7**, 309–339.

Gerstenberger, H., 1989. Autometasomatic Rb enrichments in highly evolved granites causing lowered Rb–Sr isochron intercepts. *Earth and Planetary Science Letters* **93**, 65–75.

Harley, S. L., 1989. The origin of granulites: a metamorphic prospective. *Geological Magazine* **126**, 215–247.

Heinrich, C. A., 1982. Kyanite eclogite to amphibolite facies evolution of hydrous mafic and pelitic rocks, Adula Nappe, Central Alps. *Contributions to Mineralogy and Petrology* **81**, 30–38.

Hodges, K. V. & Spear F. S., 1982. Geothermometry, geobarometry and the Al_2SiO_5 triple point at Mt. Moosilauke, New Hampshire. American Mineralogist **67**, 1118–1134.

Hofmann, J., Mathe, G. & Wienholz, R., 1981. Metamorphose und zeitliche Stellung tektonometamorpher Prozesse im östlichen Teil des Saxothuringikums. *Zeitschrift für geologische Wissenschaften* **9**, 1291–1308.

Holdaway, M. J., 1971. Stability of andalusite and the aluminium silicate phase diagram. *American Journal of Science* **271**, 97–131.

Holland, T. J. B., 1980. The reaction albite = jadeite + quartz determined experimentally in the range 600–1200°C. *American Mineralogist* **65**, 129–134.

Hoth, K., Lorenz, W. & Berger, H. J., 1983. Die Lithostratigraphie des Proterozoikums im Erzgebirge. *Zeitschrift für angewandte Geologie* **29**, 413–418.

Johannes, W., 1984. The significance of experimental studies for the formation of migmatites. In: Ashworth, J. R. (ed.) *Migmatites*. Glasgow: Blackie, pp. 36–85.

Klápová, H., 1990. Eclogites of the Bohemian part of the Saxothuringicum. *Rozpravy Ceskoslovenske Akademie Ved, Rada Matematickych a Prirodnich Ved* **100**, 1–86.

Klemm, I., 1995. Druck–Temperaturentwicklung von Metamorphiten im östlichen Erzgebirge (Sachsen). Unpublished Diploma Thesis, Ruhr-Universität Bochum, 121 pp.

Kossmat, F., 1916. Über die Tektonik des Gneisgebietes im westlichen Erzgebirge. *Zentralblatt für Mineralogie, Geologie und Paläontologie* **1916**, 135–144.

Kossmat, F., 1925. Erscheinungen und Probleme des Überschiebungsbaus im variskischen Gebirge Sachsens und der Sudetenländer. *Zentralblatt für Mineralogie, Geologie und Paläontologie* **1925**, 348–359.

Kotková, J., 1993. Tectonometamorphic history of lower crust in the Bohemian Massif example of north Bohemian granulites. *Czech Geological Survey Special Papers* **2**, 42 pp.

Kotková, J., Kröner, A., Todt, W. & Fiala, J., 1996. Lower Carboniferous HP event in the Bohemian Massif: evidence from North Bohemian granulites. *Geologische Rundschau* **85**, 154–161.

Koziol, A. M. & Newton, R. C., 1988. Redetermination of the anorthite breakdown reaction and improvement of the plagioclase–garnet–Al_2SiO_5–quartz geobarometer. *American Mineralogist* **73**, 216–223.

Krentz, O., Thomas, R. & Wiedemann, R., 1990. Aussagen zur Regionalmetamorphose des mittleren und westlichen Erzgebirges mit Hilfe thermobarometrischer Einschlußuntersuchungen. *Zeitschrift für geologische Wissenschaften* **18**, 315–326.

Krohe, A., 1992. Krustendehnung im Erzgebirge? Ansatze zu einem neuen Konzept. *Zentralblatt für Geologie und Paläontologie* **1992**, 180 (abstract).

Krohe, A., 1997. Variscan tectonics of Central Europe: postaccretionary intraplate deformation of weak continental lithosphere. *Tectonics* **15**, 1364–1388.

Kroll, H., Evangelakis, C. & Voll, G., 1993. Two-feldspar geothermometry: a review and revision for slowly cooled rocks. *Contributions to Mineralogy and Petrology* **114**, 510–518.

Kröner, A. & Willner, A. P., 1995. Magmatische und metamorphe Zirkonalter für Quarz–Feldspat-Gesteine der Gneis–Eklogit-Einheit des Erzgebirges. *Terra Nostra* **95**(8), 112.

Kröner, A., Willner, A. P., Hegner, E., Frischbutter, A., Hofmann, J. & Bergner, R., 1995. Latest Precambrian (Cadomian) zircon ages, Nd isotopic systematics and *P–T* evolution of granitoid orthogneisses of the Erzgebirge, Saxony and Czech Republic. *Geologische Rundschau* **84**, 437–456.

Kryza, R., Pin, C. & Vielzeuf, D., 1996. High-pressure granulites from the Sudetes (south-west Poland): evidence of crustal subduction and collisional thickening in the Variscan Belt. *Journal of Metamorphic Geology* **14**, 531–546.

Kurze, M., 1966. Die tektonisch-fazielle Entwicklung im Nordostteil des sächsischen Lineamentes. *Freiberger Forschungshefte* **C201**, 1–58.

Le Go , E. & Ballèvre, M., 1990. Geothermobarometry in albite–garnet orthogneisses: a case study from the Gran Paradiso nappe (Western Alps). *Lithos* **25**, 261–280.

LeBreton, N. & Thompson, A. B., 1988. Fluid-absent (dehydration) melting of biotite in metapelites in the early stages of crustal anatexis. *Contribution to Mineralogy and Petrology* **99**, 226–237.

Lorenz, W. (compiler), 1982. Metallogenetisches Kartenwerk 1:100 000. Geologische Karte Erzgebirge/Vogtland. Berlin: Zentralinstitut für Geologie.

Lorenz, W. & Hoth, K., 1990. Lithostratigraphie im Erzgebirge—Konzeption, Entwicklung, Probleme und Perspektiven. *Abhandlungen des Staatlichen Museum für Mineralogie und Geologie zu Dresden* **37**, 7–35.

Massonne, H.-J., 1991. High-pressure, low-temperature metamorphism of pelitic and other protoliths based on experiments in the system K_2O–MgO–Al_2O_3–SiO_2–H_2O. Unpublished Thesis of Habilitation, Ruhr-Universität Bochum, 172 pp.

Massonne, H.-J., 1992. Thermochemical determination of water activities relevant to eclogitic rocks. In: Kharaka, Y. K. & Maest, A. S. (eds) Water–Rock Interaction. *Proceedings of the 7th International Symposium on Water–Rock Interaction, Park City, Utah*. Rotterdam: Balkema, pp. 1523–1526.

Massonne, H.-J., 1994. *P–T* evolution of eclogitic lenses in the crystalline complex of the Erzgebirge, Middle Europe: an example for high-pressure to ultrahigh-pressure metabasites incorporated into continental crust. *Extended abstract 1. Workshop on Ultra-high-pressure Metamorphism and Tectonics, Stanford, CA, USA*. Stanford: School of Earth Sciences, pp. A29–A32.

Massonne, H. J., 1995. Experimental and petrogenetic study of UHPM. In: Coleman, R. G. & Wang, X. (eds) *Ultrahigh Pressure Metamorphism*. Cambridge: Cambridge University Press, pp. 33–95.

Massonne, H.-J. & Grosch, U., 1995. *P–T* evolution of Paleozoic garnet peridotites from the Saxonian Erzgebirge and the Aheim region, W. Norway. *Extended abstract, Sixth International Kimberlite Conference, Novosibirsk*. Stuttgart: Schweizerbart, pp. 353–355.

Massonne, H.-J., Grosch, U. & Willner, A. P., 1993. Geothermobarometrie mittels Ti-Gehalten in Kalihellglimmern. *Berichte der Deutschen Mineralogischen Gesellschaft, Beiheft 1 zum European Journal of Mineralogy* **5**, 85.

McMullin, D. W., Berman, R. G. & Greenwood, H. J., 1991. Calibration of the SGAM thermometer for pelitic rocks using data from equilibrium experiments and natural assemblages. *Canadian Mineralogist* **29**, 889–908.

Mehnert, K. R., 1968. *Migmatites and the Origin of Granitic Rocks*. Amsterdam: Elsevier.

O'Brien, P. J. & Carswell, D. A., 1993. Tectonometamorphic evolution of the Bohemian Massif: evidence from high pressure metamorphic rocks. *Geologische Rundschau* **82**, 531–555.

O'Brien, P. J., Kröner, A., Jaeckel, P., Hegner, E., Zelazniewicz, A. & Kryza, R., 1997. Petrological and isotopic studies on Palaeozoic high pressure granulites with medium pressure overprint, Góry Sowie (Owl) Mts., Polish Sudetes. *Journal of Petrology* (in press).

Reinisch, R., 1929. Erläuterungen zur Geologischen Karte von Sachsen, Nr. 129, Blatt Zöblitz, 2nd edition [1st edition by Hazard (1884)]. Leipzig: Geol. Landesamt Sachsen.

Rötzler, J., 1992. Zur Petrogenese im sächsischen Granulitgebirge. Die pyroxenfreien Granulite und die Metapelite. *Geotektonische Forschungen* **77**, 1–100.

Rötzler, K., 1995. Die *PT*-Entwicklung der Metamorphite des Mittel- und Westerzgebirges. Scientific Technical Report STR95/14, Geoforschungszentrum Potsdam, 220 pp.

Rötzler, K., Schumacher, R. & Maresch, W. V., 1993. *PT*-Entwicklung in Glimmerschiefern und Orthogneisen des Westerzgebirges. *Berichte der Deutschen Mineralogischen Gesellschaft, Beiheft 1 zum European Journal of Mineralogy* **5**, 257.

Scheumann, K. H., 1935. Die Rotgneise der Glimmerschieferdecke des sächsischen Granulitgebirges. *Abhandlungen der sächsischen Akademie der Wissenschaften, mathematisch–naturwissenschaftliche Klasse* **87**, 251–286.

Schmädicke, E., Okrusch, M. & Schmidt, W., 1992. Eclogite-facies rocks in the Saxonian Erzgebirge, Germany: high pressure metamorphism under contrasting *P–T* conditions. *Contributions to Mineralogy and Petrology* **110**, 226–241.

Schmädicke, E., Mezger, K., Cosca, M. A. & Okrusch, M., 1995. Variscan Sm–Nd and Ar–Ar ages of eclogite facies rocks from the Erzgebirge, Bohemian Massif. *Journal of Metamorphic Geology* **13**, 537–552.

Schreurs, J., 1985. Prograde metamorphism of metapelites, garnet–biotite-thermometry and prograde changes of biotite chemistry in high grade rocks of West Uusimaa, Southwest Finland. *Lithos* **18**, 69–80.

Sebastian, U., 1995. Die Strukturentwicklung des spätorogenen Erzgebirgsaufstiegs in der Flöhazone—Ein weiterer Beitrag zur postkollisionalen Extension am Nordrand der Böhmischen Masse. Doctoral Thesis, TU Bergakademie Freiberg, 100 pp.

Seltmann, R., Bankwitz, P. & Hösel, G., 1991. Structural environment of tin granites in the Erzgebirge. In: Pagel, M. & Leroy, J. L. (eds) *Source, Transport and Deposition of Metals*. Rotterdam: Balkema, pp. 493–496.

Steltenpohl, M. G., Cymerman, Z., Krogh, E. J. & Kunk, M. J., 1993. Exhumation of eclogitized continental basement during Variscan lithospheric delamination and gravitational collapse, Sudety Mountains, Poland. *Geology* **21**, 1111–1114.

Vielzeuf, D. & Pin, C., 1989. Geodynamic implications of granulitic rocks in the Hercynian belt. In: Daly, J. S., Cli , R. A. & Yardley, B. W. D. (eds) Evolution of the Metamorphic Belts. *Geological Society Special Publications* **43**, 343–348.

Von Quadt, A., 1993. The Saxonian Granulite Massif: new aspects from geochronological studies. *Geologische Rundschau* **82**, 516–530.

Werner, O., Hess, J. C. & Lippolt, H. J., 1996. Das variscische Abkühlungsmuster des Westerzgebirges—Ergebnisse isotopischer Mineraldatierungen. *Terra Nostra* **96**(2), 192–196.

Wienholz, R., Hofmann, J. & Matte, G. 1979. Über Metamorphose, Tiefenbau und regionale Position des Erzgebirgskristallins. *Zeitschrift für geologische Wissenschaften* **7**, 385–395.

Willner, A. P., 1994. Chlor in metamorphen Biotiten—Ein Überblick. *Berichte der Deutschen Mineralogischen Gesellschaft, Beiheft 1 zum European Journal of Mineralogy* **6**, 312.

Willner, A. P., Rötzler, K., Maresch, W. V., Krohe, A. & Kopp, J., 1993. Hochdruckrelikte und Druck–Temperatur-Entwicklung in Orthogneisen des mittleren Erzgebirges. *Berichte der Deutschen Mineralogischen Gesellschaft, Beiheft 1 zum European Journal of Mineralogy* **5**, 256.

Willner, A. P., Rötzler, K., Krohe, A., Maresch, W. V. & Schumacher R., 1994. Druck–Temperatur–Deformations-Entwicklung verschiedener Krusteneinheiten im Erzgebirge. Eine Modellregion für die Exhumierung von Hochdruck-Gesteinen. *Terra Nostra* **94**(3), 104–106.

Willner, A. P., Klemm, I., Rötzler, K. & Maresch, W. V., 1995. Petrologische Belege aus dem mittelkrustalen Niveau für eine variskische Krustenstapelung im Erzgebirge. *Terra Nostra* **95**(8), 138.

Willner, A. P., Kröner, A. & Teufel, S., 1996. Time of formation, peak of HP-metamorphism and cooling history of quartz–feldspar rocks from the Central Erzgebirge (Saxony/Germany). International Goldschmidt Conference, Heidelberg, *Journal of Conference Abstracts* **1**, 675.